CHALMERS

Experimental and Analytical Simulation of MFCI (Molten Fuel Coolant Interaction) during CDA (Core Disruptive Accident) in Sodium Cooled Fast Reactor

Master of Science Thesis in the Masters Program, Nuclear Engineering

VENKATARAMAN NATARAJAN

KARTHIK RAVICHANDRAN

Department of Applied Physics

CHALMERS UNIVERSITY OF TECHNOLOGY

Göteborg, Sweden, 2011

CTH-NT-252 ISSN 1653-4662

Experimental and Analytical Simulation of MFCI (Molten Fuel Coolant Interaction) during CDA (Core Disruptive Accident) in Sodium Cooled Fast Reactor

Master of Science Thesis in the Masters Program, Nuclear Engineering

VENKATARAMAN NATARAJAN

KARTHIK RAVICHANDRAN

Department of Applied Physics

CHALMERS UNIVERSITY OF TECHNOLOGY

Göteborg, Sweden, 2011

CTH-NT-252 ISSN 1653-4662

ABSTRACT

With increasing demand for understanding Severe Accident Scenario in Sodium Cooled Fast Reactors, there is an urgent need of enhancing numerical and experimental simulation techniques. Extensive literature survey indicates complete data but firm conclusions on molten coolant interaction and their consequent effects of fragmentation and settlement behaviour on core catcher is not available comprehensively. Hence the entire phenomena of settlement of molten core debris on the core catcher are described by defining individual phenomenon associated with this scenario. These phenomena include expulsion of molten fuel from the cladding and its interaction with sodium. These phenomena are important to understand MFCI effects on pin failures. This is the pre-disassembly phase in CDA. The order of pressure developed and the associated temperature would govern pin-pin interaction and ultimately leading to melting of sub-assembly phenomena. In this aspect it is highly important to know the phenomena of molten fuel in liquid sodium. In the post accident phase, entire fuel melts and its relocation occurs inside the core. During the relocation, the molten fuel comes into contact with the structures inside the core which leads to fragmentation. Due to this numerous small molten particles are created which interacts with sodium. The integrated effects of these particles are required to determine the loading on the vessel. The transport phenomena of the molten fuel in the core and its settlement behaviour are also analyzed in the post accident phase. In order to analyze these phenomena, sophisticated experimental facility is needed to validate the numerical simulation. This thesis deals with the analytical simulation of the pressure, temperature rise and the transport behaviour of a single particle. To understand the complexity involved in performing this experiment, a small scale experimental facility is constructed at IGCAR and preliminary data are generated. The input data from these basic phenomena can be used for developing and validating international codes like SAS4, SIMMER. A possible approach for addressing the re-criticality phenomenon is proposed in this thesis and a model calculation is also done. This model analysis yields a situation which seems conducive for re-criticality to occur. Even though our analysis takes into account the effect of a single particle reacting with sodium which might not lead to a potential consequence in the point of re-criticality, for asserting the safety of such situation, the approach proposed must be validated and developed further in order to accurately claim the probability of the situation in realistic condition with large amount of fuel.

Acknowledgement

- ***We thank our examiner Anders Nordlund for all his support and guidance throughout the thesis tenure.***
- ***We thank IGCAR for giving us the opportunity to work with them.***
- ***We thank our Supervisor and Guide in the organization Dr.P. Chellapandi for his continuous support and technical guidance which helped us complete our thesis successfully.***
- ***A special thanks to all the Scientists at SED/IGCAR for helping us to complete the thesis.***

Contents

List of Abbreviations

SFR	*Sodium Cooled Fast Reactors*
FSR	*Fast Spectrum Reactors*
PFBR	*Prototype Fast Breeder Reactor*
LMFBR	*Liquid Metal Cooled Fast Breeder Reactor*
BDBA	*Beyond Design Basis Accident*
CDA	*Core Disruptive Accident*
UTOPA	*Unprotected Transient Over Power Accident*
ULOFA	*Unprotected Loss of Coolant Accident*
PAHR	*Post Accident Heat Removal*
MFCI	*Molten Fuel Coolant Interaction*
MOX	*Mixed Oxide Fuel*
PIE	*Postulated Initiating Event*
SS	*Stainless Steel*
SOFI	*Sodium Coolant Interaction Facility*
PATH	*Post Accident Thermo Hydraulics Facility*

CHAPTER 1

Introduction:

Nuclear power contributes to 6% of world's energy and approximately 15% of world's electricity supply[14]. Plutonium is generated during reactor operation and large quantities have been collected and dumped in the repositories from 5 decades of reactor operations. Due to this, environmental pollution, safety and security concerns have been raised in the recent years. To address these issues and to take necessary action, the plutonium dumped is converted into reserves for further energy generation with multiple recycling. Fast breeder reactors are used for this purpose where there is minimum exchange of fuel during operation thereby avoiding excess exploitation of the reserves. Till recently, there have not been demands for power production from SFR. Due to raising pollution concerns and increasing power demand, Sodium cooled Fast Reactors comes into existence significantly. International collaborations have been made in order to construct and commission these SFRs and to create awareness about the role of fast reactors in the future. The key points addressed for SFR operation are the developments of the safety aspects and its adequate knowledge.

From the knowledge of the literature survey, comprehensive individual scenario definition is inadequate. Due to the nuclear renaissance, severe accident analysis has to be given highest priority and this paper makes a contribution to this analysis.

To have a better understanding of this analysis, a pool type Fast Breeder Reactor is taken as a basic system. This report concentrates on the following sections:

1. Description of pool type fast reactor system focussing on the core
2. Safety aspects and Severe Accident Scenario of Fast Reactors
3. Literature survey to bring out numerical and experimental simulation. The main aim of the literature survey is to derive conclusions and thereby to derive the need for Research & Development
4. Theoretical Analysis
5. Experimental simulation- fuel melting and challenges faced
6. Future research opportunities
7. Discussion and Conclusion

CHAPTER 2- Prototype Fast Breeder Reactor

Description of Prototype Fast Breeder Reactor:

In India, the uranium reserves are very modest (~100 kilo tonnes). Fast spectrum reactors (FSR) are essential and important due to effective utilisation of natural uranium with breeding. With FSR, the available uranium can feed 275 GWe for about 200 years, when used after reprocessing. Available thorium can feed 275 GWe capacity power plants for about 550 years. Apart from efficient utilization of uranium, the FSR is an efficient system for converting thorium to ^{233}U required in the third stage. Sodium cooled fast reactors (SFR), in particular, would provide critical liquid metal technology and high temperature design inputs for the accelerator driven systems, fusion and high temperature reactor systems. They can also provide electricity at competitive costs over long periods. Hence, the development of SFRs has been given high emphasis and the SFR programme is growing steadily without any interruption since 1972, irrespective of international scenario.

PFBR is a pool type reactor with 2 primary and 2 secondary loops with 4 steam generators per loop. The overall flow diagram comprising of primary circuit housed in reactor assembly, secondary sodium circuit and balance of plant (BoP) is shown in Figure 1. The nuclear heat generated in the core is removed by circulating sodium from cold pool at 670 K to the hot pool at 820 K. The sodium from hot pool after transporting its heat to four intermediate heat exchangers (IHX) mixes with the cold pool. The circulation of sodium from cold pool to hot pool is maintained by two primary sodium pumps and the flow of sodium through IHX is driven by a level difference (1.5 m of sodium) between the hot and cold pools. The heat from IHX is in turn transported to eight steam generators (SG) by sodium flowing in the secondary circuit. Steam produced in SG is supplied to turbo-generator.

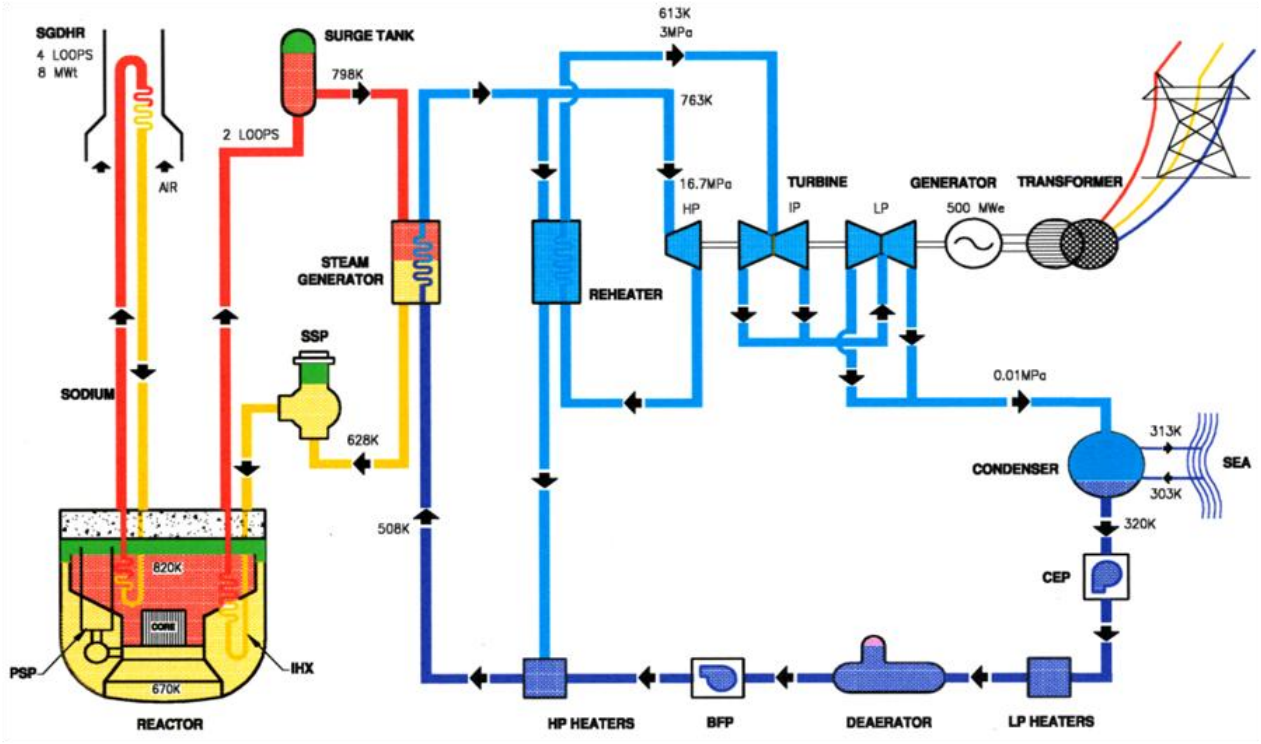

Figure 1: PFBR flow sheet [15]

In the reactor assembly (Figure 2), the main vessel houses the entire primary sodium circuit including core. Liquid Sodium is filled in the main vessel with free surfaces blanketed by argon. The inner vessel separates the hot and cold sodium pools. The reactor core consists of about 1757 subassemblies including 181 fuel subassemblies. The control plug, positioned just above the core, houses mainly 12 absorber rod drive mechanisms. The top shield supports the primary sodium pumps, IHX, control plug and fuel handling systems. PFBR uses mixed oxide with both natural and depleted uranium, 21 % Pu oxide in the inner core and 28% Pu oxide in the outer core. For the core components, 20 % cold worked D9 material (15 % Cr- 15 % Ni with Mo and Ti) is used to have better irradiation resistance. Austenitic stainless steel type 316 LN is the main structural material for the out-of-core components and modified 9Cr-1Mo (grade 91) is chosen for SG. PFBR is designed for a plant life of 40 y with a load factor of 75 %.

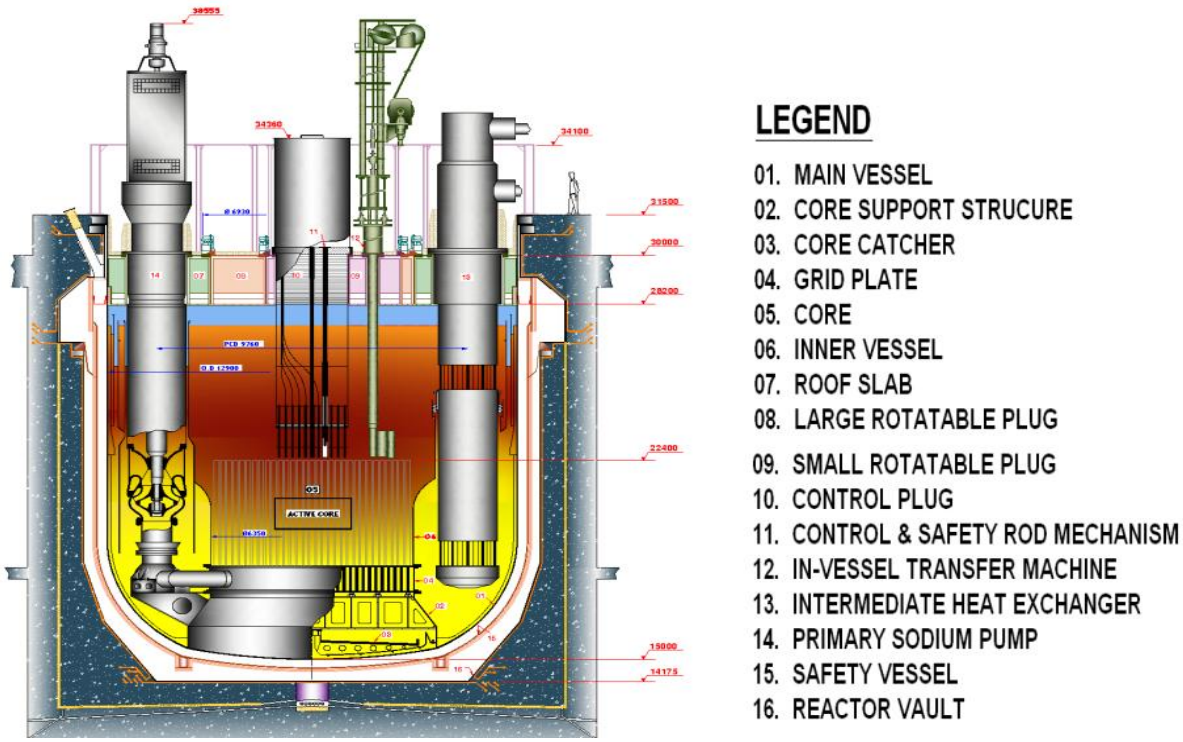

Figure 2: Schematic of PFBR Assembly [15]

FSRs have many inherent features, such as lower values of delayed neutron fraction (β), shorter neutron generation time (l) and non-reactive core configuration etc, which are claimed to be disadvantages for fast reactors. However, from the internal safety report [15] they do not pose truly any significant disadvantages. The benefits are derived from the fast and continuous reactivity feedback by the Doppler (enhanced neutron absorption cross sections due to temperature) and fuel expansion. In SFR, large margin between the normal operating sodium temperature and the boiling point of sodium can accommodate significant temperature rise in the event of mismatch between heat generation and heat removal. High thermal conductivity, low viscosity and large difference between the temperature of hot sodium at 820 K and ambient air at 310 K, coupled with significant variation of sodium density with temperature, permit decay heat removal through natural convection mode. Further, in particular, pool type concept provides large thermal inertia and hence, more time for the operator to act in case of exigencies during reactor operation. Temperature and power coefficient of reactivity are negative. So in the event of disturbances in primary and secondary sodium flows or feed water flow, the reactor stabilizes to a new power level even without the corrective action of the operator. The potential initiators of coolant boiling are prevented by incorporating special design features. The temperature changes are measured accurately at the core outlet with very small time delay, employing fast response thermocouples so that at the right time, counter measures are possible. Many engineered safety features are introduced in the fast reactor system for ensuring the fuel cladding integrity, core coolability and reliable reactor shutdown and decay heat removal capabilities. The issues related to sodium chemical reactions, though treated comprehensively starting from sensor development to technology, need further research and development.

CHAPTER 3- Severe Accident Scenario

3.1 Safety features of FBR:

In the water reactor, the core is in its most reactive configuration and hence, any phenomenon that results in disintegration of core makes the reactor, generally, to shutdown automatically. This is not the case with SFR. The disintegration of core in SFR (fuel slumping for example) may lead to power excursion, resulting in an accident. The core has high density of power, which can have a positive voiding effect. The physio-chemical characteristics of sodium pose sodium water reaction and chemical toxicity challenges. There is a need for development of specific and innovative technologies for in-service inspection of the structures under sodium due to opaqueness of sodium. Repairing circuits and components in post-accidental situation call for sophisticated and specific technologies. The SFR components, i.e. large size thin walled shell structures, are also sensitive to earthquake loadings. The requirement of high breeding ratio, burning of minor actinides in suitable matrices and enhanced safety with improved economy needs advanced materials and technologies which call for extensive experimental, modelling and simulation technologies. High burn-up targeted for the future reactors and near complete burning of minor actinides and long lived fission products introduce higher levels of radioactivity during fuel handling and fuel reprocessing.

Fast reactors are generally designed to be stable and the experiences accumulated so far have demonstrated the attainability of such stability. Even though potential for the radiation release to atmosphere exists during accident, there are numerous inherent and engineered safety features to inhibit such a kind of radiation release mentioned in the internal safety report [15]. High quality materials, matured design, high construction and inspection standards, guides and methodologies lead to robust design for the core and coolant circuits. This design philosophy has the ultimate objective of minimising or eliminating the initiators which lead to partial or whole core meltdown. Design provisions such as diversity in shutdown and decay heat removal systems are introduced to meet the safety limits with adequate margins for the design basis events, so as to prevent beyond design basis events. Advanced design features for the management of beyond design basis events include prevention of re-criticality in molten core by way of having effective core catcher and containment. In order to demonstrate the safety, analysis is performed by postulating various scenarios of high probability to very low probability. The events which result in the highest damage is commonly labelled the beyond design basis accident (BDBA). Beyond the DBA, there lies a domain of accident consequences which are less probable and in order for such accident to take place, at least two or more low probability failures must take place in sequence, e.g., a large reactivity insertion event coupled with complete failure of the plant protection system. These BDBA which involves degradation or melting of whole core is termed as Core Disruptive Accident (CDA) or Severe Accidents.

In addition to the above safety features, there are there physical barriers which confine the radioactive material at specified locations preventing it from entering the outside environment.

1. The fuel matrix itself- normally a ceramic material has considerable capability for retaining solid fission products as well as gaseous fission products in the unrestrained region.
2. The fuel pin cladding
3. The primary coolant system

The fourth barrier is the outer containment represents an engineered safeguard.

3.2 CDA: Phenomenology

The severe accident scenarios resulting in CDA in sodium cooled fast reactors (SFR) are (1) unprotected loss of flow with subsequent transient overpower causing bulk core melting, criticality events and mechanical energy release, (2) local blockage resulting in melt propagation from one subassembly to neighbouring subassemblies, (3) slow power transients causing core melting and recritcality, (4) failure of post accident heat removal systems causing recriticality and vessel integrity and (5) large source term uncertainty resulting in release of unacceptable fission products.

A mismatch between heat generation and heat removal in the core can occur if either the heat generated is more than the heat removal, or the heat removal is less than the heat generated. The former situation occurs if uncontrolled reactivity insertion occurs leading to corresponding power increase. The latter situation will rise if there is coolant flow starvation and inadequate heat removal. With accompanying shutdown system failure, the former situation is termed as Unprotected Transient Overpower Accident (UTOPA) and the latter is termed as Unprotected Loss of Flow Accident (ULOFA). Apart from this, if there is a failure in heat removal system, the situation is termed as Protected Loss of Heat Sink Accident (PLOHSA). In UTOPA scenario, initially the fuel melts. This leads to in-pin fuel motion which itself acts as a shutdown mechanism. If the positive reactivity excursion continues, it can then result in clad failure, Na voiding and Core collapse. In ULOFA initially coolant voids which is followed by clad failure. This ultimately results in fuel slumping. Core collapse or slumping can induce positive reactivity and produce CDA where lot of thermal energy is released due to neutronic power excursion. Subsequent core dispersal reduces core reactivity and terminates the highly energetic phase of the accident.

Uncontrolled reactivity addition leading to UTOPA can occur due to: (a) uncontrolled withdrawal of control rods, (b) passage of large bubble in core and (c) collapse of core support structure leading to core compaction. Uncontrolled withdrawal of control rods is a PIE, even though control rods are usually moved for a pre-planned distance. If the worth of the rod is high

enough or more than one rod is involved, it can lead high reactivity addition and consequent large power increase. Uncontrolled reactivity addition can also occur due to passage of large gas bubble in the core. Passage of such a large gas bubble in the core in very highly unlikely and the reactivity that can be inserted in present designs (with low coolant void reactivity effect) is low. Small gas bubbles result in very negligible reactivity addition. UTOPA can perhaps occur due to sudden structural failure of core support structure which is again considered as residual risk at present. The core support structure is a safety class 1 component with a box type structure and random failures or stiffeners do not degrade its performance. Structural vibrations caused by seismic excitations can give rise to only reactivity oscillations, which are small in magnitude (less than 0.5 $, which a peak pulse), and further there is damping due to negative reactivity feedbacks and which can be shown to result in only a small increase in reactor power. Hence, the uncontrolled withdrawal of control rod is the only initiator considered for UTOPA and possible CDA.

The coolant flow starvation can be initiator for ULOFA, caused by failure of primary pump or seizure of primary pump or pipe rupture or total instantaneous blockage in subassembly. The failure of primary pump due to loss of power supply can be an initiator for CDA. The loss of power supply leads to flow coast down (with flow halving time of about 8s to 10s) and reduced heat removal, leading to mismatch in heat balance. The pipe rupture does not lead to total flow starvation. Total Instantaneous blockage is prevented by having multiple holes for coolant entry in the foot of subassembly and an adapter at the top of the subassembly gives an alternate flow path. Pump seizure can lead to a CDA, if it does not recover operation within in a few tens of seconds. Thus, the pump seizure or stoppage of primary pump due to loss of power supply is the only main initiator for ULOFA and possible CDA.

3.3 Different Phases of a CDA:

CDA analysis is carried out extensively with the ultimate measure of how the main vessel and top shield responds to the mechanical energy release. For this analysis, various stages have to be considered with an initiating event. The mechanical energy release during the accident is estimated and the response given by other physical structures have to be analysed. The CDA consists of 3 phases.

Pre-disassembly phase:

In this phase the accident initiation leads to 1) neutronic shutdown with essentially intact geometry, 2) a gradual core meltdown and 3) the onset of conditions for hydrodynamic core disassembly due to generation of high internal pressures from vaporized core materials.

The analysis in this phase that are performed are calculations for core neutronics, reactivity feedbacks, thermal hydraulics, sodium boiling, fuel pin failure, cladding and fuel slumping together with their relocation and fuel coolant interaction.

Transition phase:

At the end of the predisassembly phase, the reactor can become subcritical or the fuel and clad can melt and form a molten pool. The former situation happens when there are sufficient negative reactivity feedbacks resulting in termination of the accident. The latter situation arises when there are insufficient negative reactivity feedbacks. The fuel transforms from solid phase to liquid phase gradually and hence it is called as transition phase. The core can boil and then cool down leading to sub critical configuration or criticality condition can reoccur.

Disassembly phase:

Once the fuel starts dispersing, fuel displacement feedback dominates, and all other reactivity feedbacks except Doppler can be ignored. The time scales are in the order of milliseconds for these feedbacks. The core subsequently loses its integrity and this phase continues till the reactor attains sub-criticality due to fuel dispersal. The core neutronics and core hydrodynamic calculations are performed for the dispersing core in this phase.

3.4 Mechanical and Thermal Consequences of CDA:

During the pre-disassembly phase, the overheating occurs due to power excursion leading to melting of the core. This heating will generate vapour phase in subsequent stages which has a high potential to cause mechanical load due to its high pressure and temperature. The mechanical energy release is due to the expansion of vapour phase from initial pressure P_0 which is at saturated condition to final pressure P_f equal to ambient condition prevailing in the reactor. During the rapid expansion of the core bubble in the liquid sodium environment which is considered as isentropic, pressure or shock waves are generated which deform the shell structures surrounding the core. Subsequent to completion of mechanical work, the vapour phase which is at ~ 5000 K, condenses due to cooling of sodium pool which is at 855 K and starts moving downwards melting the support structures, such as grid plate and core support structure. Finally, the liquid settles on the core catcher and subsequently will be cooled by natural convection.

The different phases of CDA are shown in Figure 3.

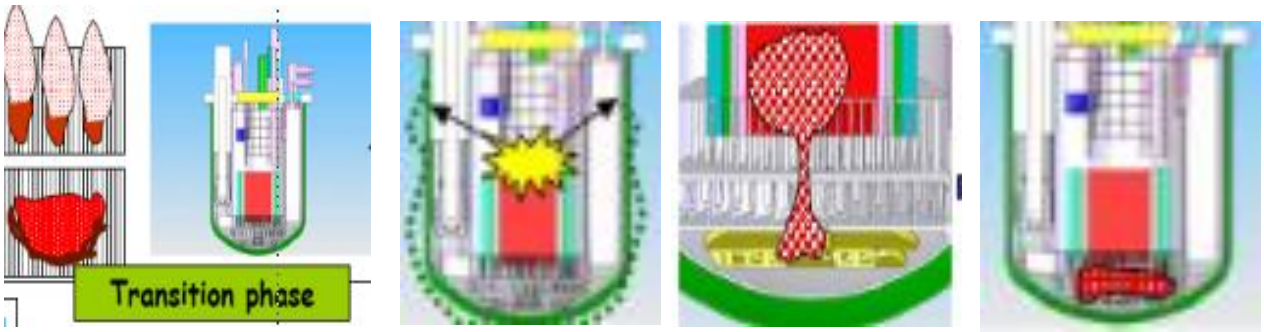

Melting and vaporisation of core (a) | *Mechanical energy release (b)* | *Molten fuel relocation (c)* | *Post accident heat removal (d)*

Figure 3: Different phases of CDA [15]

3.5 Post Accident Phase:

The capability of achieving a stable coolable material configuration following the postulated accident is demonstrated by appropriate objective of post accident heat removal (PAHR) mechanisms. The distribution of heat sources following the accident is a controlling factor in the assessment of adequacy of PAHR. Because of the substantial differences in the accident scenario, the post accident dispersion behaviour also varies. The PAHR analysis should therefore be prepared to cover a range of possible fuel distribution patterns. Analysis of the UTOPA shows that the early sweep out of fragmented fuel may limit the damage in the core to few subassemblies. However, scenario following a ULOFA may result in gross whole core melt down. In such a case, sufficient steel and fuel vapour may be generated in the core to result in fuel removal from the core, within a two phase mixture of fuel and steel, thus leading to neutronic shutdown. The exact amount of fuel that will be driven into the cold plenum of the reactor vessel cannot be predicted. Therefore, to define the pattern of fuel dispersal following a CDA in an SFR, from the reference [15] a semi-mechanistic approach is currently being pursued.

CHAPTER 4- Literature Survey

Literature Survey of MFCI (Uranium and sodium) Experiments:

A.W.Cronenberg and H.K.Fauske [1] conducted an experiment to study the phenomenon of UO_2 solidification associated with rapid cooling in liquid sodium in 1974. According to the author, the kinetics of crystal formation and growth are investigated and compared with the heat transfer controlled solidification rate to determine whether or not the surface of UO_2 droplet can remain molten if contact is established during quenching in sodium coolant. Prior to this experimentation, in an attempt to explain such type of fragmentation phenomenon, a number of models had been advanced with different assumptions on the physical state of the sample surface at the time of break up. The shell theory states that, the entrapped coolant undergoes vaporization and pressurization leading to shell failure while the thermal stress theory states that the quenching conditions of UO_2 in sodium are such as to produce thermal gradients large enough to cause material yielding and break-up. Similarly theories like the violent boiling, cavitation and Helmholtz instability states that the material is readily deformable and undergoes fragmentation due to pressure forces generated at the surface or internally in the case of acoustic cavitation model. In his analysis the kinetics of the crystal nucleation and growth are determined. This was then compared with UO_2 heat transfer process where solidification is controlled by the rate at which the latent heat can diffuse through the solid layer. The author has also reviewed the heat transfer process, rate of crystal growth and super cooling between solidifying UO_2 and sodium. The position of the liquid solid interface obtained from the heat transfer process theory was translated into an interface velocity function and this heat transfer controlled solidification velocity is then compared with the rate of solid growth determined from crystallization theory. From the crystallization theory, the rate of crystallization was determined as the function of sub-cooling, independent of S-L interface condition but the experimental results indicate that a liquid can exist for a long time at a temperature well below it freezing point without crystal inception. Thus A.W.Cronenberg and H.K.Fauske[1] concluded that the UO_2-sodium contact temperature is well below the homogenous crystallization temperature and that the estimated rate of crystal growth (71cms/sec at T_I) is larger than the heat transfer controlled solidification velocity for time greater than 1ms, indicates that solidification commences immediately after contact and is limited by the heat transport process. From the calculations carried out, the limiting condition of the UO_2-Na quenching process can be established which guarantees oxide fuel freezing. Assuming that the UO_2 surface must be cooled to its homogenous crystallization temperature to ensure solidification, the sodium bulk temperature may be as high as 1870 degree. In reality, however, the coolant temperature may be greater if heterogeneous nucleation is initiated by the presence of foreign materials. However, the fact remains that only at UO_2 temperatures well below the homogenous crystallization point will the molecular motion be retarded to the extent that the average rate of the crystal growth is less than the heat transfer governed solidification velocity. It is therefore concluded that in the analysis of fuel fragmentation in LMFBR system, the effect of surface solidification should be accounted for.

Hiroshi MIZUTA [2] conducted an experiment to analyze fragmentation of UO_2 after molten UO_2 –Na interaction in 1974. The author conducted a series of experiments where 30 runs were performed to gain information on the fragmentation of molten UO_2 when dropped into a bath of liquid sodium. In this experiment, the UO_2 pellets were heated with electric current. High-speed cinematography (~2000 fps) was used to observe the fragmentation phenomenon of UO_2 droplets on impact with sodium. He examined the physical characteristics (particle size distribution, particle shape and surface condition and microstructure) of solid UO_2 particles resulting from the quench, to gain an insight into the mechanism of fragmentation. Figure 4 shows the sequence of events during the impact of the UO_2 droplet on the sodium surface and its subsequent fragmentation. From his experiments he concludes that the impact of UO_2 droplets on the sodium surface cause extensive fragmentation of the droplets, but generated only feeble pressure pulses in the liquid bath. The occurrence of the pressure pulses would appear to have been governed by droplet surface temperature and higher peak pressure is correlated with finer particle size. Droplets with its surface solidified during its free fall would still be liable to extensive fragmentation. Upon immersion in the sodium bath, the entire droplet is instantly cooled to sodium temperature and their solid-liquid fragmentation at this instant determines the particle size distribution. In performing safety analysis of fuel-coolant interaction, the author assumes that the UO_2 droplets would form spherical particles and the resulting particle size distribution would be log-normal. He concludes that the characteristics of UO_2 particles during its free fall appear to play an important role in subsequent fragmentation mechanism.

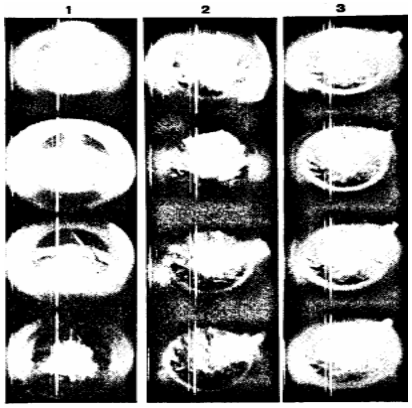

Figure 4: Sequence of events during impact of the UO_2 droplet on the sodium surface

Roland B.Knapp and Neil E.Todreas [3] carried out an analytical study to determine the applicability of the concept of thermal stress fragmentation to the UO_2-sodium fuel-coolant interaction in 1975. The authors states that major emphasis were put on the fracture mechanics approach to assess whether or not solidifying UO_2 would fracture under the thermally induced stresses. It was found that the stress levels were sufficient to generate the k_I values substantially in excess of the UO_2 fracture toughness k_{IC}. This work was directly concerned with the possible FCI accident situation in an LMFBR system where the fuel is UO_2 and coolant is liquid sodium. Therefore the main concern was whether or not such interaction of large quantities of molten fuel and coolant will result in rapid pressurization coupled with the development of the local shock

wave. This analytical study was then initiated in an effort to confirm the thermal stress fragmentation hypothesis via fracture mechanics approach. The efforts were specifically directed towards determining the applicability of the mechanism, and if so, to what range of conditions of applicability are, the time history of the process and how it compares with experiments. The model that was employed for the analysis that was carried out was that of a molten spherical droplet instantaneously immersed in an infinite coolant pool. Based on the postulated contact interface boundary condition, approximate thermal approximations were employed to determine the values of the solidification rate and the temperature distribution within the solidifying shell. The crux of the analysis centres on the knowledge of the fracture toughness of the fuel k_{IC} and local stress intensity factor. The simplified requirement for fracture was then written as $k_I \geq k_{IC}$. To conduct the thermal analysis two basic modes were employed where the first method was based on the steady state solution of London and Seban while the second method was used by Adams approximation [12] for the case of fixed surface temperature. Then second method was also used by Cronenberg in his studies. Finally, Roland B.Knapp and Neil E.Todreas concluded that throughout the analysis, during UO_2-Na thermal interaction the stresses generated in the solidifying shell were sufficient to result in fracture from anticipated inherent flaws. By extending the analysis to Al_2O_3 the studies also concluded that the validity of the thermal stress fragmentation theory is limited to semi-brittle or brittle materials. The overall process of analytical modelling is not complete. An overall prediction of probabilistic flaw distribution, crack initiation and propagation, and overall time scale for complete interaction requires definition and evaluation. Other minor factors requiring assessment include the growth stability under the influence of thermal stresses alone. Clarification of these factors and an improved overall model will then provide an accurate estimate of the time to fail and subsequent particle size distribution for incorporation into the existing parametric accident analysis models.

H.Schins and F.S.Gunnerson [4] analyzed the boiling and fragmentation behaviour during fuel-sodium interactions in 1985. The authors provide the following information for better understanding of their motive. The experiments were performed in BETULLA I and BETULLA II facilities. The fuels were copper and stainless steel which had initial temperatures far above the melting points and urania and alumina with their melting temperature as the initial temperature. The boiling behaviour was analyzed keeping the concepts of nucleate boiling, film boiling and transition boiling as background information as shown in the following Figure 5.

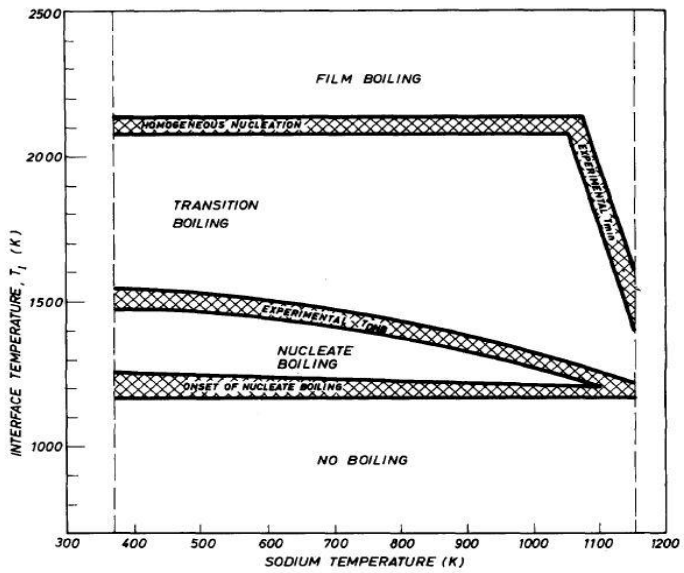

Figure 5: Concept of Nucleate, transition and film boiling [4]

Prior to this experiment, there are evidences showing that for molten metals like stainless steel or copper, the resultant debris particles were physically smooth whereas for oxide fuels like urania or alumina, the debris particles were fractured. The experiment was first conducted using the BETULLA I facility where 4kg of molten UO_2 at 2850^0 C was dropped into liquid Na pool whose temperature was between 350 and 700^0 C. The fall guide tube is 4m long. 8 pressure transducers are installed in the wall of the reaction tank which was actually developed in the laboratory for operations up to 800^0C. UO_2 temperature was measured by optical pyrometers. BETULLA II facility had some alterations in the fuel release mechanism, the guide tube and the interaction vessel. The guide tube was shortened to 0.875m. The sodium content in this facility is 3.4kg. The instrumentations include a pyrometer to assess the temperature of the crucible, a photocell to indicate the passage of molten fuel droplets or jets, several chromel-alumel thermocouples to monitor the temperature evolution within the sodium pool, a pressure transducer in the argon head for measuring potential energetic events and a pressure transducer in the sodium to measure associated pressure spikes. From the test results, the authors conclude by stating the fact that transition boiling is the dominant mode of thermal energy exchange upon fuel contact with subcooled sodium. The authors also state that unlike fuel-water interaction, an initial period of stable film boiling is difficult to attain in fuel-sodium systems. According to their analysis, two fragmentation mechanisms dominate for the oxide fuels. The first is the prompt and rapid fragmentation of molten fuel due to boiling induced hydrodynamic forces. This mechanism produces the characteristic smooth and spherical frozen fuel particles. The second is delayed thermal stress mechanism which gives rise to the fractured particulate. There was no energetic event that resulted in all the 13 molten fuel-subcooled sodium tests. Such observations may suggest that initial transition boiling precludes favourable pre-mixing conditions necessary for a coherent, energetic event.

J.D.Gabor, R.T.Purviance, R.W.Aeschlimann and B.W.Spencer [5] conducted tests in which break-up behaviour of kilogram quantities of molten uranium, uranium-zirconium alloy, and uranium-iron alloy pour streams in 600 degree Celsius sodium was studied in 1988. The uranium metals were melted inductively with a TOCCO motor generator for this experiment. The authors conclude saying that the tests did not produce any vapour explosions due to the interactions because the conditions were far from satisfying vapour explosion criteria. The following are also the conclusion from their research. The particle size also decreased with increased duration of the hydrodynamic action on the pour stream before freezing. The largest particles obtained were from the tests with low melt temperatures. Tests with sodium depth of 0.3m the pour streams broke up and the fragments solidified before reaching the bottom of the interaction vessel. The rapid achievement of thermal equilibrium is reflective of the high thermal conductivity of uranium metal and sodium. It is thus evident from calculations that were performed based on typical bed conditions observed in tests that the debris from the meltdown of metal-fuel pool reactor would be largely coolable by conduction alone without considering the enhanced heat removal by convection. Several correlations for the maximum boiling heat flux before dry out of deep beds were compared for a representative particle size of 10mm, and all constantly showed that for 0.9m voidage the bed depth were extra-ordinarily high. Even for a bed of 0.5 voidage the entire core with no stainless steel at bottom spherical surface of a reactor with a 6m radius would be coolable. Hence, on the metal fuel pour stream breakup and coolability that in-vessel retention would be the most likely outcome.

Satoshi Nishimura, Izumi Kinoshita, Ken-ichiro Sugiyama and Nobuyuki Ueda [6] conducted some tests in 2002 to verify the thermal fragmentation of molten jet dropped into the sodium pool at instantaneous contact interface temperatures below freezing point. Some details given by the authors regarding the analysis have been comprehensively given in the following part. The experiments were carried out using molten copper and sodium. In the experiment 20 grams of copper was melted in a crucible with an electric heater and was dropped through a 6mm nozzle into a sodium pool of 553K in the form of jet column. Thermal fragmentation originating inside the molten copper jet with a solid crust was clearly observed in all the test runs. It was verified that a small quantity of sodium which is locally entrapped inside the molten jet due to the organized motion between the molten jet and sodium, is vaporized by the sensible heat and latent heat of molten copper and the high internal pressure causes the molten jet with a solid crust to fragment. It is also found that the fragmentation caused in the molten copper-sodium interaction was severer than that of molten uranium alloy jet-sodium interaction which was reported by Gabor et al., under the same superheating condition and lower ambient Weber number condition of molten copper. Figure 6 illustrates the organized motion between the coolant and molten jet. From these experiments the conclusions reached by the authors were that the thermal fragmentation originating inside the molten copper jet with a solid crust was clearly observed. It is verified that the fragmentation of molten copper jet with a solid crust is caused by internal pressure produced by the boiling of sodium which is locally entrapped inside the molten

jet due to the organized motion between the molten jet and coolant. It is also confirmed that the amount of powder like fragments effectively increases with increasing superheating of molten copper jets even under the condition that instantaneous contact interface temperatures are below the freezing point. The increasing tendency of the amount of fine fragments in the present study is qualitatively consistent with the results of molten copper jets obtained at superheating of higher than 800K. It was also found from the comparison of the fragment size distributions in the different mass and geometric scales that the fragmentation caused in the molten copper-sodium interaction was severer than that in the molten uranium alloy jet-sodium interaction under the same superheating condition and lower ambient Weber number condition of molten copper. The effect of initial temperature of molten jet on fragment size distributions is as shown in Figure 7.

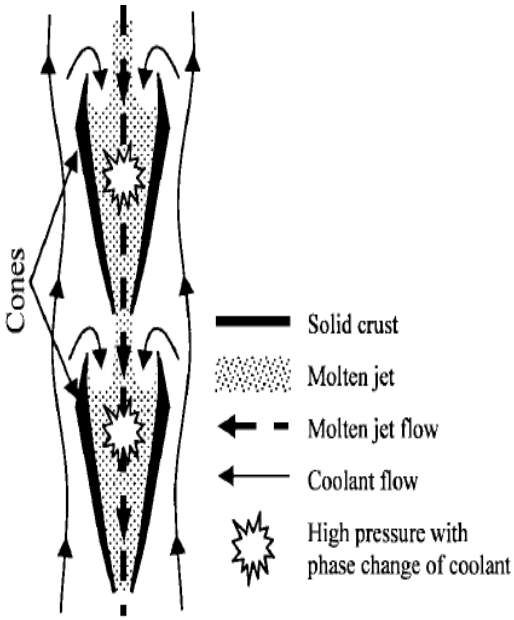

Figure 6: Schematic diagram of organized motion between coolant and molten jet with solid crust

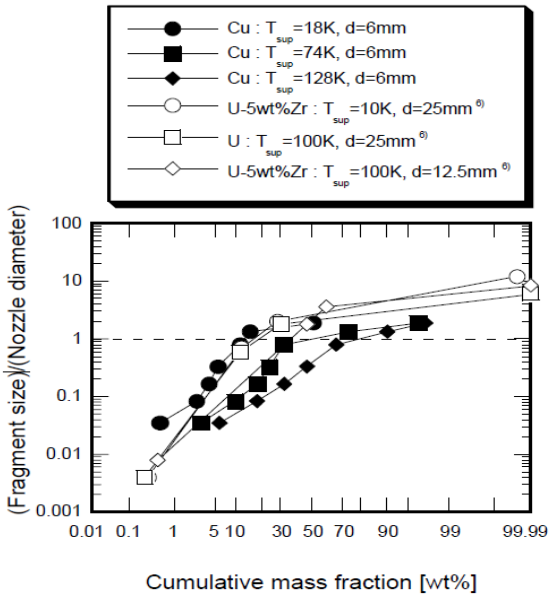

Figure 7: Effect of initial temperature of molten metal fuel and copper on fragment size distributions as per the tests conducted. [6]

Eiji Matsuo, Yutaka Abe, Keiko Chitose, Kazuya Koyama and Kazuhiro Itoh [7] in 2007, performed experiment to study the jet break up behaviour at core disruptive accident for fast breeder reactor. The analysis, experiment carried out and the conclusions from the authors can be found briefly in the following lines. U-alloy78 (mixture of U, Bi, In, Sn metals) [7] was used as the simulant for core material and it was injected into water which was used as the simulant for coolant. The simulant materials were selected in such a way that the relation of the density between U-alloy78 and water is near the relation between MOX fuel and Na coolant. The objective of this experiment was to clarify the dominant effect on the jet break up behaviour and the fragmentation to evaluate the cooling possibility of the molten jet in coolant during core disruptive accident. The visual data of the molten jet breakup behaviour is observed by using the high-speed video camera. After the experiment, the solidified fragments were collected and the mass median diameter was measured. A quench model to estimate the cooling possibility during a CDA of a FBR was constructed, reflecting the results of the experiments. Previous studies prior to this experiment shows that the jet break up behaviour in another immiscible fluid can be categorized into three modes, namely, deformation, boundary layer stripping and surface waves instability caused by Kelvin-Helmholtz instability or Rayleigh- Taylor instability. Many experiments and models done with various simulants suggest that Kelvin-Helmholtz instability is the likeliest reason for jet breakup. The authors have discussed various theories for break up and fragmentation. Saito's correlation and Epstein's correlation describes the breakup phenomenon while Rayleigh-Taylor instability, Critical Weber number theory and Kelvin-Helmholtz instability discusses the phenomena for fragmentation. Figure 8 shows the typical observation results of the molten jet behaviour. The molten jet front velocity was estimated by calculating the differentiation of the locations. Figure 9 and Figure 10 shows the jet front location and velocity

respectively. From the experiments it was found that the velocity of molten jet front can be divided into three regions. From the observations made in the experiment, the jet breakup length was defined as the distance from the water surface to the location between region I and II (where the jet column disappears). The jet breakup length was determined by the duration of region I. Thus, there was a possibility that jet breakup length depended on the initial molten jet column diameter, that is, the injection nozzle diameter. Figure 11 shows the influence of the nozzle diameter on the jet breakup length and hence it shows that jet breakup length is not influenced by jet penetration velocity. From the above observations and results it was speculated that the dominant effect of the jet breakup behaviour is fragmentation on the jet side due to the shear force by the relative velocity. The experiment was followed by a modelling to estimate the cooling possibility during a CDA of a FBR. This model was applied to PAHR evaluation for a typical FBR condition. From the results, the authors conclude by stating that the jet column disappears as soon as the jet front velocity suddenly decreases. The jet breakup length depends on the injection nozzle diameter and not on the jet velocity. Figure 12 shows the plot of Jet break-up length vs Jet penetration velocity. The tendency was equal to Epstein's equation. The median diameters of the solidified fragment are located near critical Weber number theory and the most unstable wavelength. It has been suggested that the quench behaviour is enhanced due to the increase of the jet velocity, since the fragment diameter becomes small. If the jet breakup length was to depend on the jet velocity as described by Saito's equation then more of the molten material jet would reach the floor. For applying the present experimental results to the situation of PAHR at a CDA of a FBR, further analysis to estimate the effects such as molten fuel coolant interaction and the possible surface solidification of molten fuel when the molten oxide fuel contacts the sodium coolant must be performed.

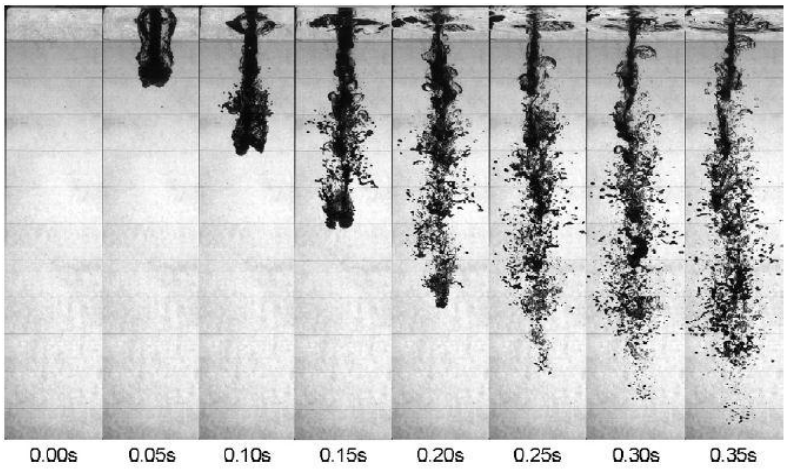

Figure 8: Typical observation results of the molten jet behaviour [7]

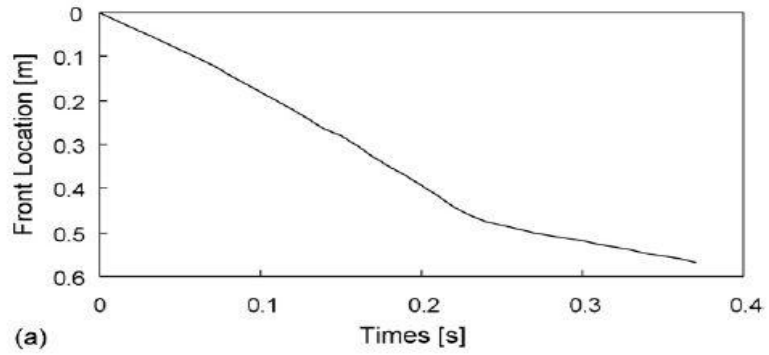

Figure 9: Time vs Jet front location [7]

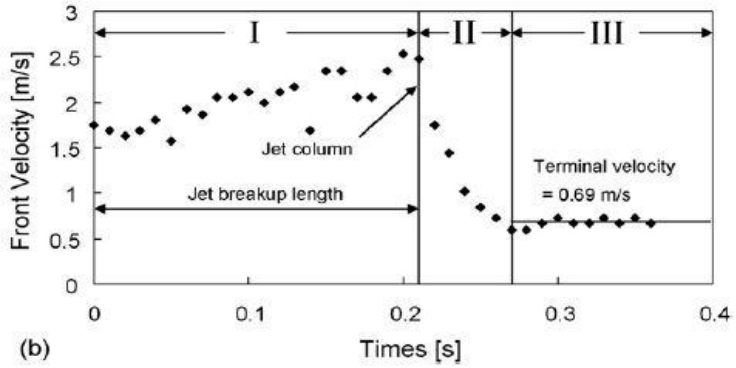

Figure 10: Time vs Jet front velocity [7]

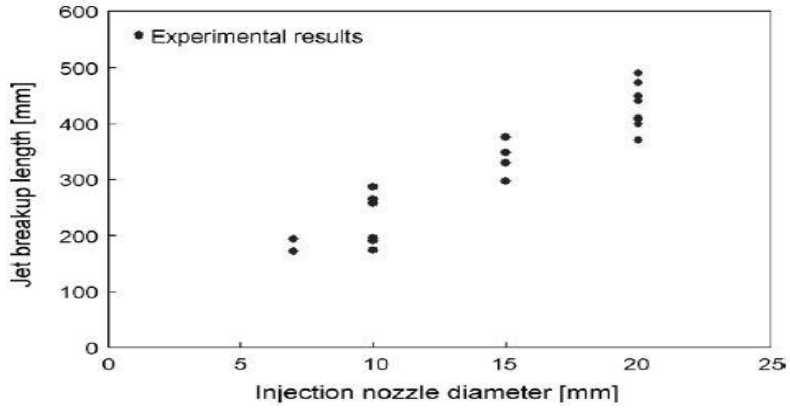

Figure 11: Influence of nozzle diameter on the jet break up length [7]

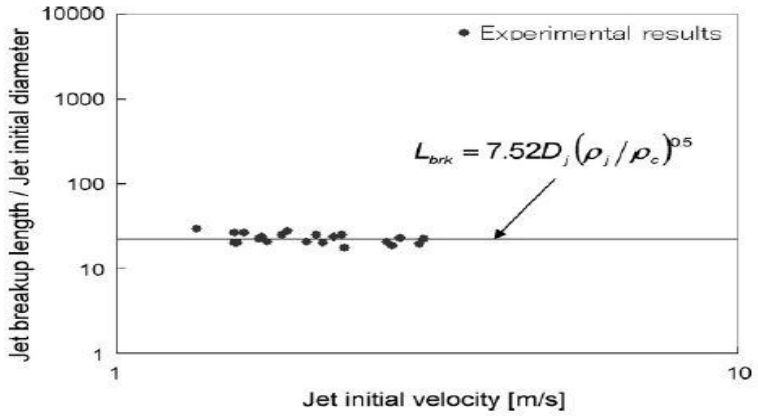

Figure 12: Jet break-up length vs Jet penetration velocity [7]

Conclusions derived from Literature Survey are as follows:

1. Limited number of experiments with respect to Uranium and Sodium.
2. The CDA scenario includes specific individual phenomenon like relocation of molten fuel, transportation, solidification, fragmentation and settlement. Papers explaining such fundamental phenomenon are inadequate.

From the conclusion, few interesting phenomena and the challenges associated in conducting experiments are addressed without focussing on any linkage.

CHAPTER 5- Interface film pressure

5.1 Calculation of Interface film pressure during Uranium- Sodium interaction:

An MFCI phenomenon is said to occur when molten fuel mixes with the sodium in such a manner that the rate of heat transfer from the fuel to the sodium coolant is much faster that the rate which occurs during normal boiling and the major consequence of such an interaction is the rapid rise in the pressure due to vaporization of sodium, followed by expansion of high pressure two-phase sodium. Therefore sodium does the work on the surrounding due to this expansion. So, when molten fuel and sodium coolant are mixed, energy is instantaneously transferred as heat from the molten fuel to the coolant till thermal equilibrium is reached. In simple terms, the heat transfer from the molten fuel to the coolant takes place till both the simulants reach a common temperature. The sodium vaporizes and expands doing work on the surroundings.

Fauske [1] proposed that the following conditions are required for large scale vapour explosion.

1) Coarse premixing, allowed by film boiling.
2) Liquid-liquid contact.
3) Initial contact temperature equal to or greater than the spontaneous nucleation temperature of sodium.
4) Adequate constraints.

When two fluids are bought into contact, the interface temperature is given by the following relation.

$$T_i = \frac{(T_{hot} + \alpha T_{cool})}{(1+\alpha)} \ (K)$$

Where,

$$\alpha = \sqrt{k\rho c_{cool} / k\rho c_{hot}}$$

hot= superheated molten uranium fuel

cool= subcooled liquid sodium

T_{hot}= initial temperature of molten uranium with superheat

T_{cool}= initial temperature of liquid sodium with subcooling

k= thermal conductivity (W/mK)

ρ= density (kg/m^3)

c= specific heat capacity (J/kgK)

Therefore by using the Browning and Potter equation, the corresponding vapour pressure can be calculated for the current interface temperature. The Browning and Potter equation is given by the following relation.

$$\ln P = 11.9463 - 12633.73/T - 0.4672 \ln T$$

The major assumptions made in the calculations that are performed to determine the pressure excursions when MFCI takes place are the following. These assumptions made are highly conservative and simplifies the calculation carried out.

1) The molten fuel (uranium metal) is assumed to be a perfect sphere.
2) MFCI between the molten sphere and coolant takes place in an infinite volume of liquid sodium.

To determine the magnitude of the pressure excursion when a hot sphere interacts with an infinite volume of coolant, the theory formulated by the Louis C.Burmeister[8] is used. The theory states that when a very hot solid sphere of constant temperature is suddenly exposed to a large pool of stagnant coolant, initially a thin vapour film and non condensable gas envelops the sphere and thus there is no direct contact between the hot sphere and the coolant. As the heat transfer from the sphere to the interface is greater than the heat transfer between the interface and the liquid coolant, additional vapour film is formed. The great disparity between the densities of vapour and the liquid leads to the film's pressure to increase and to create additional space for the vapour by displacing the liquid (coolant) radially. As the liquid is displaced radially the rate of vaporization is reduced below its initial value and because of the heat flow rate from the sphere is reduced due to the increased vapour film thickness, the heat transfer rate from the interface to the coolant increases due to the dependence of saturation temperature upon pressure. Since the sphere temperature is significantly higher than the interface temperature, the temperature variation on the sphere surface over a period of elapsed time would be small and does not appreciable affect heat flow rate from the sphere. Therefore, the larger the sub-cooling of the coolant the smaller is the first pressure excursion and slower will be the increase in the vapour film thickness since the heat transfer rate from the interface to the coolant pool will be higher. Due to inertia, the liquid's radial displacement becomes too large and the total pressure in the vapour film decreases below the ambient value. The liquid then accelerates towards the sphere, and thus the total pressure, film thickness and heat flow rate are oscillatory.

In the following calculations performed the magnitude of the film's pressure first excursion is determined for the large excursions that would be expected. But to determine the magnitude of the large pressure excursion the main parameter needed would be the determination of the thickness of vapour film. The thickness of the vapour film is determined using the theoretical model developed by L.Caldarola[9] where an approximate relation is given

to determine the average value of ratio of vapour film thickness to the radius of the sphere. This relation is shown as follows.

$$y = 1.455\sqrt{\left(\mu\lambda_b/\rho_b L_{eq}\right)((T_w - \theta_s)/R_f^3 g\rho_f)}$$

and $L_{eq} = L + 0.55c_p(T_w - \theta_s)$

where,
$y = \delta_0 / R_f$

μ= viscosity of sodium vapour film

λ_b= vapour thermal conductivity

T_w= surface temperature of sphere

θ_s= saturation temperature of sodium

ρ_b= density of vapour

L_{eq}= equivalent specific heat of vapourization

R_f= radius of sphere

g= acceleration due to gravity

ρ_f= density of fuel(kg/m^3)

c_p= vapour specific heat capacity at constant pressure

1 dyne= 10^{-5}N

1erg= 10^{-7}J

L = latent heat of vaporization.
c_p = specific heat capacity of vapour at constant pressure

5.1.1 Calculation procedure:

Assumptions:

- The fuel is assumed to be spherical in shape.
- The radius of Uranium sphere is varied from 1mm to 30mm.
- Sodium is considered as the coolant.

- **Calculation of initial vapour pressure:**

To calculate the interface pressure during MFCI, the initial vapour pressure p_{v0} is required.

The interface temperature T_i is determined by using the relation proposed by Fauske:

$$T_i = \frac{(T_{hot} + \alpha T_{cool})}{(1+\alpha)} \ (K) \quad \textbf{(1)}$$

$$\alpha = \left(\frac{(k\rho c)_{cool}}{(k\rho c)_{hot}}\right)^{1/2} \quad \textbf{(2)}$$

Once T_i is determined, the initial vapour pressure can be found using the relation as follows. The equation gives the natural logarithm of the vapour pressure over saturated liquid sodium (liquid sodium in equilibrium with its vapour).

ln P= 11.9463-(12633.73/T_i)- 0.4672lnT_i (steady state approximation) **(3)**

The pressure thus obtained gives the value of the initial vapour pressure p_{v0}. This pressure is made non- dimensional by dividing it with P_∞.

- **Calculation of maximum film pressure excursion:**

The maximum film pressure developed during uranium- sodium interaction is derived from certain empirical relations given by Louis C. Burmeister **[8].

According to Burmeister, value of the maximum film pressure excursion is determined by the relation

$$p_m = 2/3^{1/3}\alpha^{2/3} \quad \textbf{(4)}$$

$$\alpha = \left[\frac{p_{v0}k_v(T_w - T_\infty)}{\rho_{vo}\Lambda}\right]\left[\frac{\rho R}{P_\infty \delta_0^3}\right]^{1/2} \quad \textbf{(5)}$$

where,

p_m= maximum value of p

P_∞= pressure far from sphere (bar)

p= dimensionless total film pressure = P/P_∞

p_{v0}= dimensionless initial vapour pressure = P_{v0}/P_∞

α= dimensionless parameter

k_v= vapour thermal conductivity (W/mK)

T_w= Sphere surface temperature (K)

T_∞= temperature far from sphere (K)

ρv_0= initial vapour density (kg/m^3)

Λ= heat of vapourization (J/mol)

ρ= liquid density (kg/m^3)

R= sphere radius

δ_0= initial film thickness

The value of p_{v0} is obtained from previous calculation.

Subsequently, by using the following relations, the time for the maximum film pressure excursion can be determined.

$$p_m = \left(\frac{2F^2}{e}\right)^{1/3} \quad \textbf{(6)}$$

$$\tau_m = \left(\frac{2}{F}\right)^{1/3} \quad \textbf{(7)}$$

$$t = \frac{\tau}{A} \quad \textbf{(8)}$$

$$A^2 = \frac{P_\infty}{(R\rho\delta_0)} \quad \textbf{(9)}$$

where,

F= dimensionless parameter

τ= dimensionless time = At

τ_m= value of τ at pressure's first maximum

A= parameter, $A^2 = P_\infty/R\rho\delta_0$

The parameter δ_0 in the above equation plays a significant role in the value of the peak pressure generation. This value can be assumed from various modelling papers or can be calculated using an empirical relation given by L.Caldarola [9].

$$y = 1.455\sqrt{\frac{\mu\lambda_b(T_w-\theta_s)}{\rho_b L_{eq} R_f^3 g \rho_f}} \quad \textbf{(10)}$$

where y= δ_0 / Radius of sphere

$L_{eq} = L + 0.5c_p(T_w-\theta_s)$ **(11)**

**- The relations given by Burmeister are for a hot solid sphere. Due to insufficient theory and relations for pressure excursions from a molten sphere, this theory is taken to be the base for our calculation. The latent heat part is neglected since the theory does not give accurate ideas about that. The theory is mainly dependent on temperature for the calculation and so the analysis is done by considering parameters corresponding to melt temperature.

5.1.2 Sample calculation:

Melting point of Uranium fuel= 1423K

Boiling point of sodium coolant= 1156K

Radius of Uranium sphere= 25mm

T_{hot}= 1700K

T_{cool}= 673K

The interface temperature T_i is calculated using equation (1) by using the value of α which can be determined from equation (2)

α= 0.6100 and T_i= 1310.87K

From equation (3) the value of initial vapour pressure is calculated to be **3.51 bar** and it is made dimensionless by dividing it by P_∞.

The initial vapour film thickness δ_0 is determined from (10) and (11)

δ_0= 1.17x10^{-7}m

The value of pressure's maximum excursion is determined from equation (4)

p_m= 0.0092bar (where the value of α is found from equation (5)

Subsequently, the time at which the peak pressure excursion takes place can be determined from equation (6)-(9) and it is found to be **0.229μs.**

Similar calculations are performed for various superheat and subcooling conditions. The sphere radius is also varied each time. The plot obtained is shown in Figure 13. The values of the parameters used can be found in Appendix I. The time taken for each pressure excursion can be found from Table 1 in Appendix I.

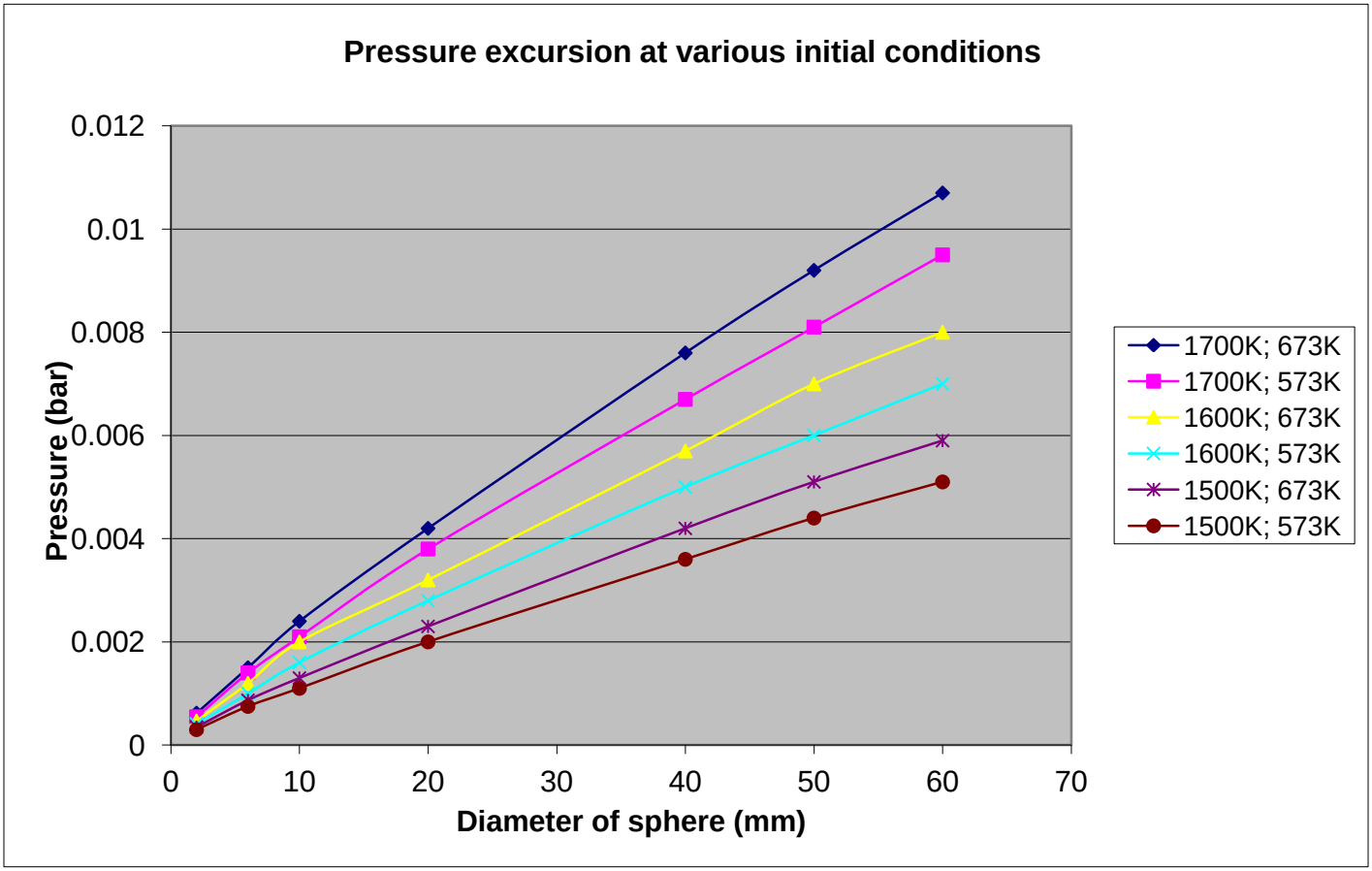

Figure 13- Pressure excursions at various initial conditions

CHAPTER 6- Particle behaviour

6.1 Determination of the time for solidification of molten Uranium droplet in Liquid Sodium and its temperature history (isothermal condition):

In both transient under-cooling (TUC) and transient over power (TOPA) accident, insufficient heat disposal occurs. This will result in overheating of the fuel and subsequent melting of the fuel rods or the whole fuel assembly. This melting will lead to a serious situation wherein the molten fuel and the sodium coolant interact. This MFCI must be properly understood in order to predict the seriousness of the situation. The pressure of the interaction must be estimated by which the stress on the surrounding components can be analyzed. The state of the melt after interaction is yet another important scenario. This final state of the melt is one stringent phenomenon for the cause of re-criticality. Therefore, to study the melt situation at the bottom of the core catcher and its settlement formation in a realistic reactor scenario, time for total solidification of the melt from the point of interaction has to be compared with the time of travel of the melt to the bottom.

At the beginning of the interaction between fuel and sodium, heat transfer occurs from the uranium fuel to the sodium coolant. The temperature of the fuel starts deteriorating whereas it starts increasing for the coolant. This process continues to the point where both the temperatures become equal and will therefore result in an equilibrium situation. Once this equilibrium point is reached, no further interaction occurs due to heat transfer. In the meanwhile, during this MFCI process, the fuel melt starts solidifying because of its temperature reaching below the freezing point. Therefore an analysis has been done in order to calculate the time for solidification of the molten metal.

Before going into a detailed analysis of the solidification part of the fuel, it would be better to have an analysis to determine the time taken to reach equilibrium condition between the fuel and coolant. This is to get a broader view of the transient process. Hence the analysis is done assuming the whole sphere is at an uniform temperature at any instant of time (isothermal condition) i.e., the temperature of the solid is spatially uniform throughout the transient process. This assumption is for simplifying the problem. The concept of lumped capacitance method is chosen due to its similar assumptions and system design. An important parameter which decides the applicability of this method is the Biot number. This Biot number is defined as the ratio of conductive resistance to convective resistance. If the value of Biot number is greater than 0.1, this method cannot be used since the error margin is higher. So making some further approximations, this method can be modified and used to determine the time for solidification.

For a molten metal to get completely converted to solid, it has to pass through two stages.

1. The '***Specific heat***' parameter reduces the temperature of the fuel from superheat condition to the freezing point of that liquid, in which no phase change occurs.

2. At the freezing point, phase change occurs by which the liquid at that temperature gets converted into solid at the same temperature. The parameter that is responsible for this process is the '***latent heat of fusion***'.

Thus for finding the complete time for solidification, the time for the temperature to reduce to freezing point from superheat and the time for phase change must be calculated and added.

6.1.1 Calculation procedure:

Assumptions:

- Droplet assumed to be spherical in shape of radius 5mm (for model calculation) in infinite sodium pool at time t=0
- The temperature of the fuel droplet is isothermal throughout the sphere at any instant of time.
- Initial conditions include
    - Fuel droplet at superheat temperature inside the infinite coolant pool at t=0
    - Sodium coolant is at a preferred sub-cooled condition
- At time t>0, the temperature of the fuel begins to drop because of the heat transfer from the fuel to the coolant. This continues till the fuel and coolant attains equilibrium temperature after which there would be no heat reduction in the fuel droplet.

The heat transfer coefficient '*h*' is assumed to take the value of 5000W/m^{2}K for sodium. This value is based on some theoretical models found in the literature. The value of '*h*' varies from 1000 to 10000W/m^{2}K (data obtained from internal safety report [15]). An average value is taken for the calculation.

Biot number $B_i = \frac{hL_c}{k}$ **(12)**

where h= heat transfer coefficient of Sodium (assumed to be 5000W/m^{2}K)

L_c= characteristic length (for sphere, it is taken as the radius for conservative approach)

k= thermal conductivity of Uranium= 60.05W/mK (from Internal safety report [15])

Substituting the above values in (12), we attain a Biot number of 0.416.

The validity of this lumped capacitance model is limited to *Bi<0.1*. Since the Biot number in the above calculation is greater than 0.1, some approximations must be adopted to calculate the time.

Using the 1-term Fourier approximation given in Incropera [10], the Fourier number can be calculated using the following approximation.

$$Fo = \frac{-1}{\varsigma_1^2} \ln \left[\frac{\theta_0^*}{C_1}\right] \quad \textbf{(13)}$$

Where Fo= Fourier number

ς_1 and C_1 are coefficients that can be determined from Table 5.1 in Incropera[10].

θ_0^*= T-T_∞/ T_i- T_∞

T_i= initial superheat temperature of molten uranium sphere (K)

T_∞= bulk temperature of sodium coolant (K)

T= temperature at any instant of time (K)

For calculation, T_i= 1700K, T_∞= 673K and for Biot number of 0.416, the coefficients C_1= 1.1200 and ς_1= 1.0677. T is reduced from 1700K till it attains equilibrium at 673K. Fourier number is determined for each value of the temperature.

The time taken for each temperature state can be calculated using a simple Fourier number definition. Fourier number is given by Fo= $\alpha t/R_0^2$. R_0 is the radius of the sphere and α is the thermal diffusivity.

α is calculated using the definition of thermal diffusivity.

$$\alpha = \frac{k}{\rho c_p} \quad \textbf{(14)}$$

where ρ= density of liquid uranium= 17300kg/m^3

c_p= 198J/kgK

Thus using the above expression, the time taken can be estimated for the whole temperature drop process. But, this time is the time taken for the temperature to drop from superheat to freezing temperature which does not take into account the time for phase change. At approximately 1400K, which is the freeing point of Uranium, phase change occurs as explained earlier.

The time for phase change is calculated using the following expression:

$$t = \frac{mL_f}{Q} \quad \textbf{(15)}$$

where L_f is the latent heat of fusion taken to be 38403.36J/kg

Q is the heat contained in the mass of fuel= mC_pdt

'm' is the mass of fuel in kg (Volume of fuel x density of fuel). Volume of a 5mm sphere is $5.23x10^{-7}m^3$.

'dt' is the difference in temperature between the freezing point of fuel and the bulk coolant temperature i.e. (1400K-673K).

According to the estimation, ***the time for the phase change is 0.83seconds***.

A plot is made for the above transient scenario between time and temperature incorporating both the times. The plot is shown in Figure 14.

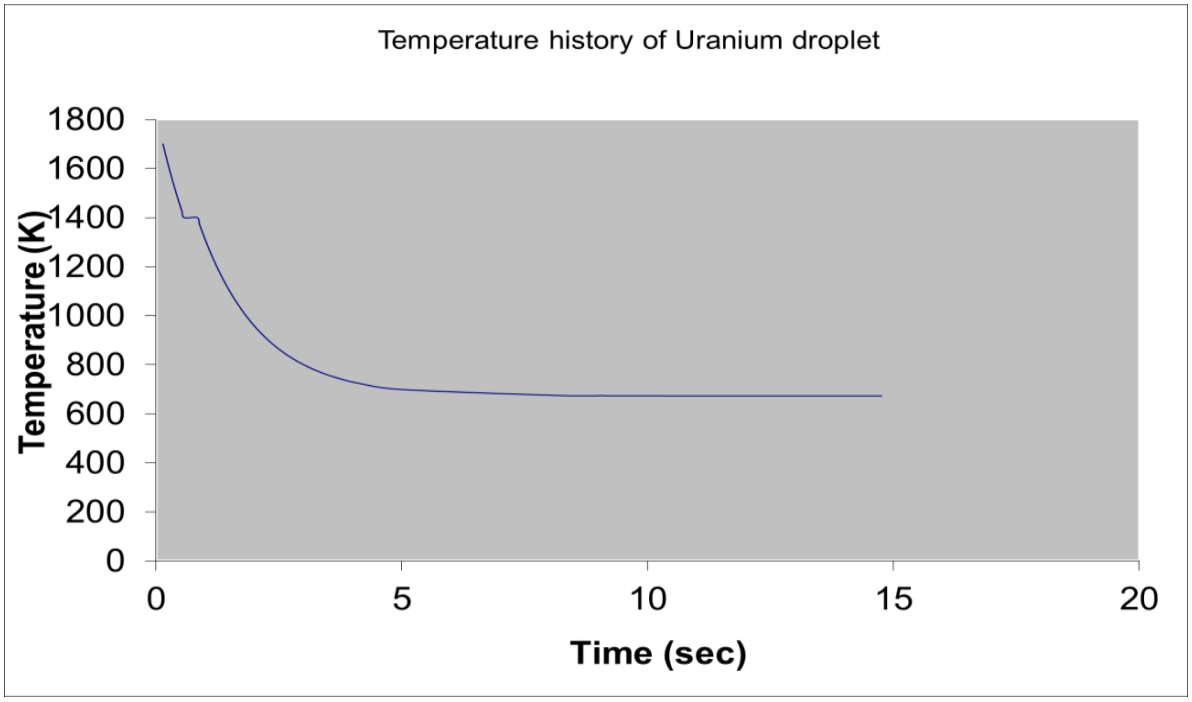

Figure 14: Temperature history of a Uranium droplet of radius 5mm.

The equilibrium temperature is obtained at around 15seconds.

The molten metal solidifies before reaching equilibrium temperature. From Figure 14, we can deduce the time for the temperature to drop from superheat to freezing point and add the time required for phase change to get the total time required for a sphere to solidify completely.

6.2 Determination of the movement of solidification front in the molten spherical droplet when it interacts with the sodium coolant:

Consider a similar accident situation as defined in the previous section. MFCI occurs and fuel starts solidifying once it reaches the freezing point. Thus here again, time taken for solidification is determined for PAHR studies. The previous time calculation is done for understanding of how the temperature profile looks when a molten sphere is cooled. In this section, the solidification analysis is done more intensely and in detail. Whenever a sphere is cooled, the outer crust solidifies before the inner regions. Thus at all the radial positions,

temperature will not be the same. The solidification happens from outer periphery to centre. Each region will be in a different state. When the outer crust is solid, may be 1mm or 2mm inside the sphere, we can find the melt yet to solidify. So it is quite helpful to investigate the movement of the solid-liquid interface within the sphere. Thus there is a time dependence of the radial temperature distribution. Again, the time for the specific heat and latent heat have to determined separately and incorporated to give the total time.

6.2.1 Calculation procedure:

Assumptions:

- Radius of the fuel droplet is assumed to be 5mm
- At time t=0, the fuel droplet is fully in contact with the sodium coolant
- At time t>0, heat transfer occurs from fuel to coolant and subsequently temperature of the fuel starts reducing. This transient process occurs till both the fuel and coolant attains equilibrium temperature.
- The solidification front (liquid-solid interface within the sphere) moves from the periphery of the sphere at r=R to the centre at r=0.

At first, the time taken for the temperature to drop from superheat temperature to the freezing point is determined in the radial direction. For this, a similar one-term approximation equation should be used as in previous section. This approximation equation contains an added parameter for the radial temperature dependence and is derived from Incropera [10].

$$\theta^* = C_1 \exp(-\varsigma_1^2 Fo) * \frac{1}{\varsigma_1 r^*} \sin(\varsigma_1 r^*) \quad \textbf{(16)}$$

where C_1 and ς_1 are constants corresponding to the Biot number as previously explained

θ^*= T-T_∞/ T_i- T_∞ (T_i= 1700K, T= 1400K, T_∞= 673K)

and r*= r/r_0 (r_0 is the radius of the molten sphere)

The parameter *Fo* contains the time‘t’ which can be estimated by changing the radius of the sphere from r=R to r=0. A graph is plotted between time‘t’ and radius of sphere (solidification front). This time represents the time for temperature to drop from superheat to the freezing point. The plot is shown in Figure 15.

The values of the parameters and the radius assumed is the same as the calculation shown in the previous section.

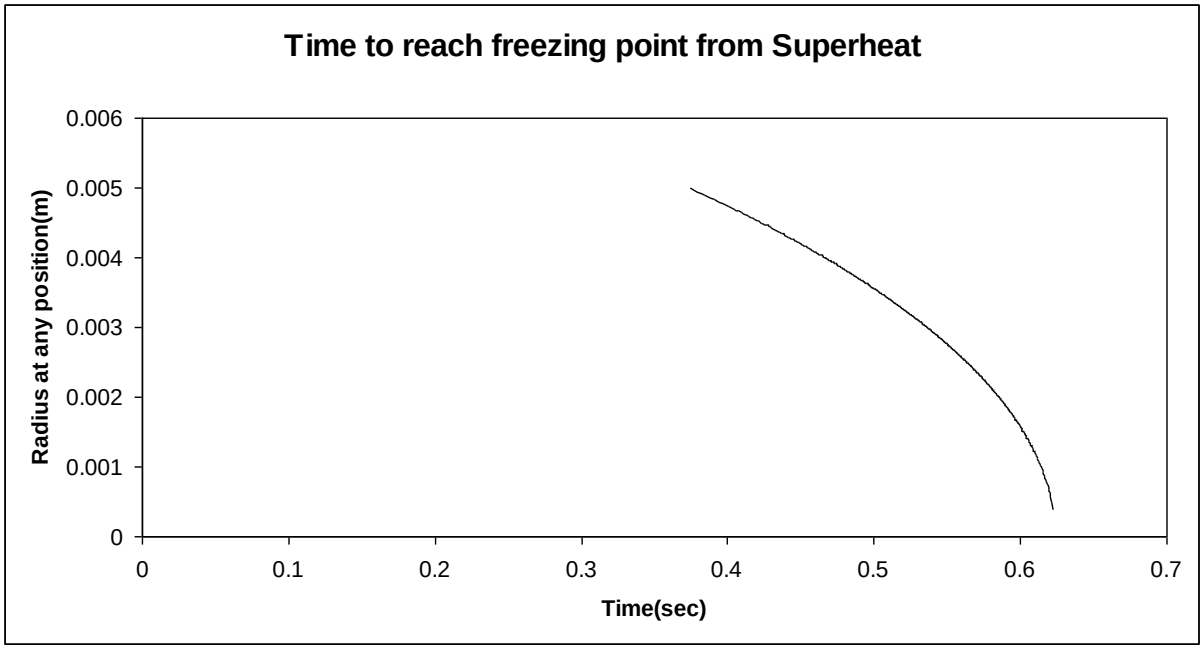

Figure 15: Time to reach freezing point from superheat for a sphere of 5mm radius

Now, the phase change process happens and the time for each of the radial position to undergo phase change is determined and plotted in Figure 16. The time for the phase change is calculated using a semi-empirical relation given by Vallet [11].

$$\frac{b-a}{b} = 1 - \{1 - \left(\frac{t}{t_s}\right)^{\frac{1}{2}} \exp\left[n\left(1 - \left(\frac{t}{t_s}\right)^2\right)\right]\}^{1/3} \quad [11] \qquad \textbf{(17)}$$

where b= outer radius of solidified shell

a= inner radii of solidified shell (solidification front boundary)

t_s= total solidification time

total solidification time 't_s' can be calculated using another relation as below

$$t_s = 0.4\frac{b^2}{h}\left(\frac{H}{c_p \Delta T}\right) \quad [11] \qquad \textbf{(18)}$$

where h= thermal diffusivity of solid metal

H= heat of fusion

c_p= specific heat of solid metal

$\Delta T = T_f - T_i$, T_f= freezing temperature and T_i= interface temperature (from (1))

The total time for solidification (phase change process for the whole sphere) is found to be 0.42seconds.

Using equation (17), the radius of the interface within the sphere is varied from periphery to centre and the corresponding time taken is found. The plot of the time for the phase change with radial dependence can be seen in Figure 16.

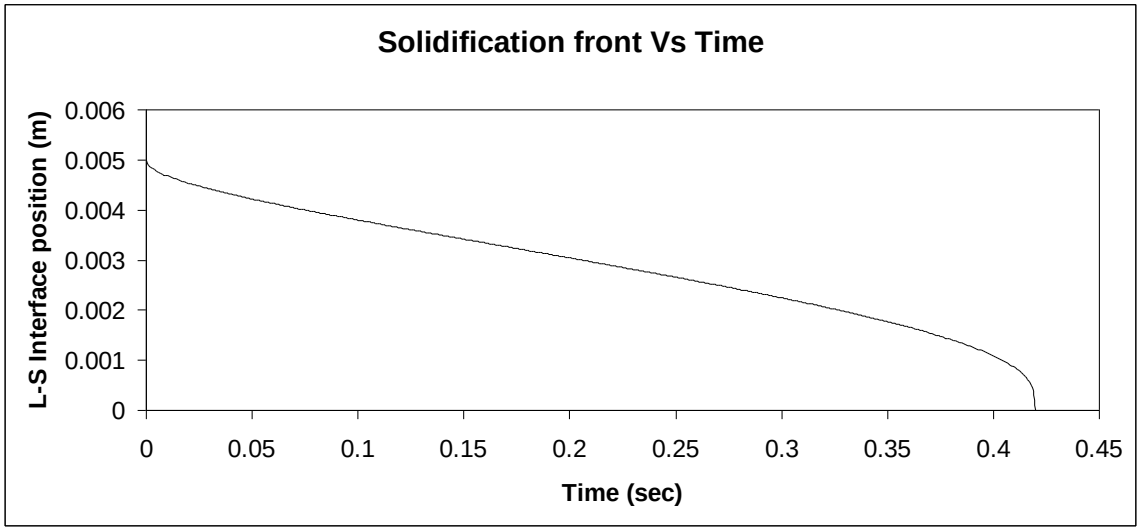

Figure 16: Time for phase change for a sphere of 5mm radius

The total time for solidification right from superheat condition till it is fully converted into a solid sphere is shown in Figure 17. Figure 15 and Figure 16 are incorporated into the same graph to show the time for total solidification at any radius of sphere.

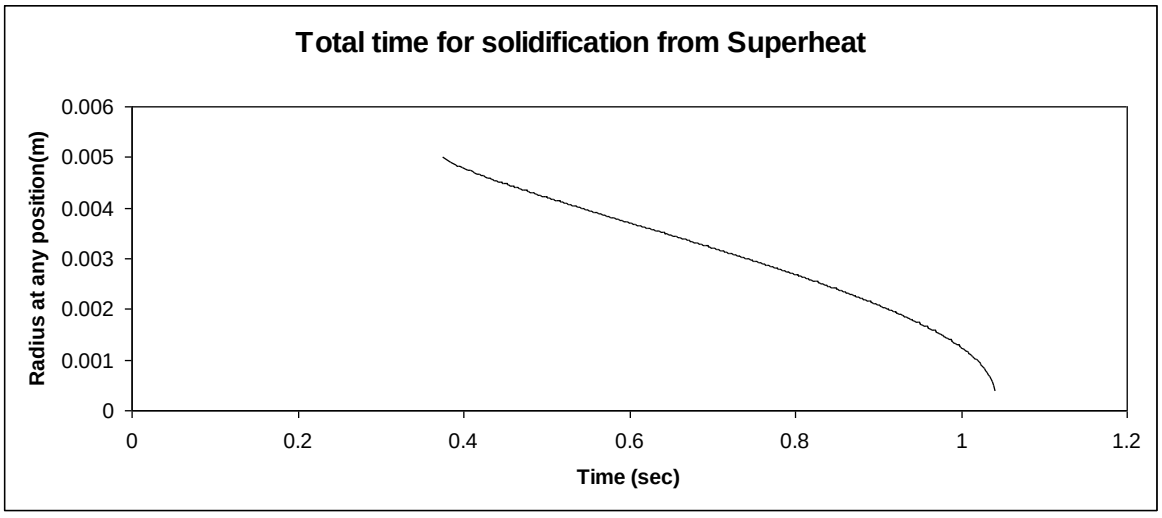

Figure 17: Total time for solidification from superheat for a sphere of 5mm radius

The solidification rate i.e. the rate at which the solid-liquid interface boundary within the sphere moves can also be deduced from an approximation solution given by C.M.Adams [12].

The approximation solution is given as:

$$\frac{da}{dt} = \frac{2h\Delta T c_p b}{a(b-a)H}\left[1 + \left(1 + \frac{4b\Delta T c_p}{3aH}\right)^{\frac{1}{2}}\right]^{-1} \quad \textbf{(19)}$$

The parameters in equation (19) are the same as previously defined in this section.

A plot is created to show the variation of solidification rate *(da/dt)* for various interface position and can be seen in Figure 18.

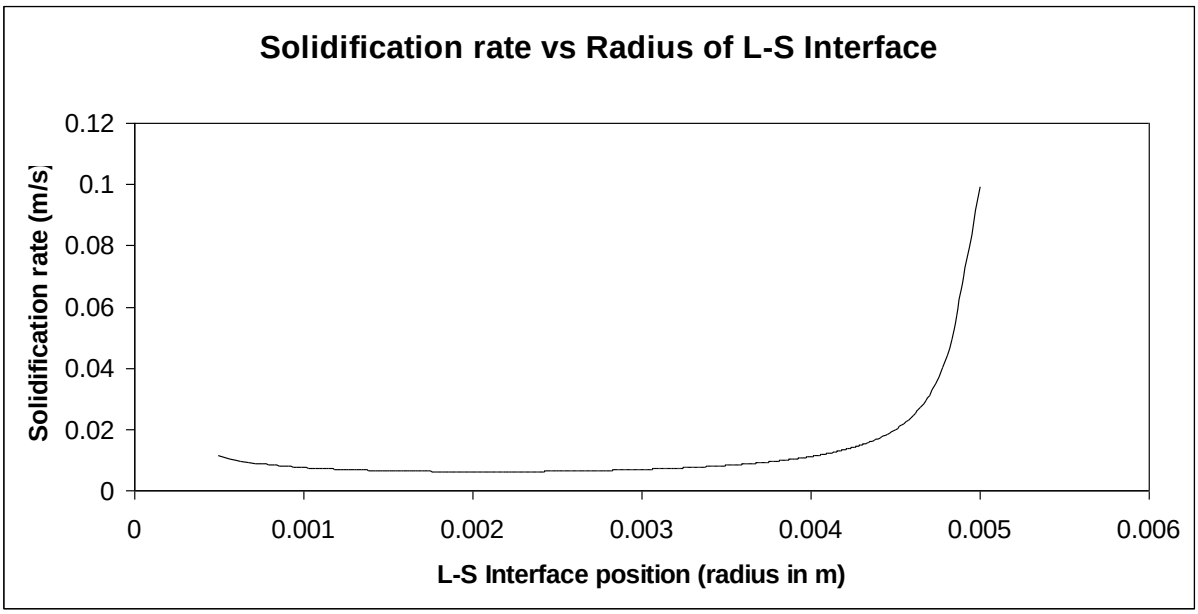

Figure 18: Solidification rate in a sphere of radius 5mm

By combining equations (17) and (19), another plot can be made to show the solidification rate variation with time. Figure 19 explains this scenario.

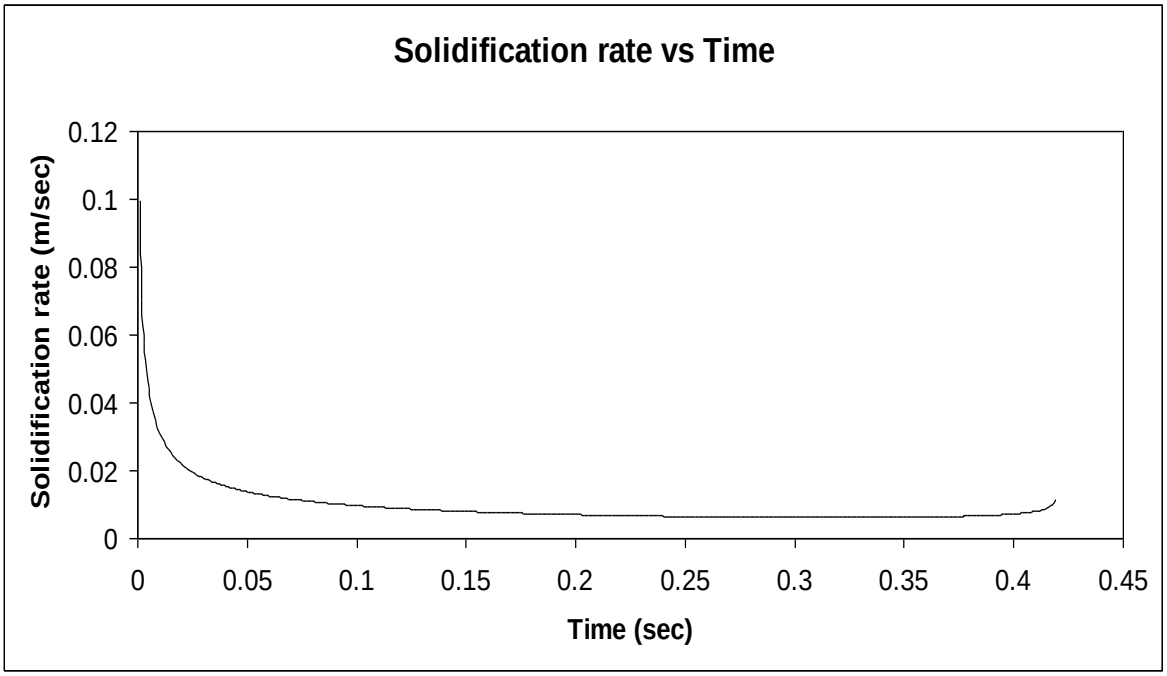

Figure 19: Solidification rate with time variation for a sphere of radius 5mm

6.3 Prediction of the state of initial molten metal sphere when it reaches the bottom of the interaction vessel after its interaction with the coolant:

One of the most vital aspects that have to be meticulously analyzed is the state of the molten metal fuel at the bottom of the core catcher after its interaction with the sodium coolant. In realistic reactor scenario, during melting of the core and its subsequent interaction with the coolant, numerous difficulties arise to control the core and its physical components from damage. The molten fuel falls into the coolant and settles at the bottom of the core catcher. It is therefore necessary to predict or approximately guess the condition of the molten core at the bottom. This is because if the state of the fuel at the bottom remains partially molten and forms a heap-shaped structure after settling, then the probability of re-criticality is high. This may lead to chain reaction with a high risk of catastrophic consequence. This risk can be avoided if the molten fuel spreads all over the core catcher and avoids the heap-shaped structure. PAHR studies have to be done in order to restrict the heat accumulation and to dispose off the heat as quickly as possible. By this way, the re-criticality is also reduced significantly.

One part of this PAHR studies include analyzing the condition of the melt at the bottom of the interaction vessel or the core catcher in case of a real reactor. The solidification time for a molten fuel particle is analyzed as explained in previous sections. In addition to this, the velocity with which the particle moves towards the bottom of the vessel is necessary. Once this speed is deduced it is quite easier to calculate the time taken for moving a particular distance. This can be compared with the solidification time to comment on the state of the melt.

A falling object attains terminal velocity if the acceleration gravity force equals the upward force of drag. In case of an object moving in a liquid, the force due to gravity is balanced by the buoyant force and the viscous force. When both forces become equal, the object attains terminal velocity. This terminal velocity should be determined in order to find the time of fall. It is assumed that for very light objects the terminal velocity will come into existence as soon as the interaction occurs between the fuel and the coolant.

Using a conservative approach, the solidification or the heat transfer in air between the melting chamber and interaction vessel is neglected and the terminal velocity is obtained at the start of the coolant surface itself.

6.3.1 Calculation procedure:

The terminal velocity is shown in equation (20).

$$V_t = \sqrt{\frac{4gd}{3C_d}\left(\frac{\rho_s-\rho}{\rho}\right)} \quad [14] \qquad \textbf{(20)}$$

where d=diameter of the sphere (m)

g=gravitational acceleration

ρ= density of fluid (kg/m^3) =860 kg/m^3

ρ_s= density of the sphere (kg/m^3) = 17300 kg/m^3

C_d= drag coefficient, usually taken as 0.47 for sphere

For the sphere of diameter 10mm, **the terminal velocity reaches 2.3m/s**.

With this value of terminal velocity, for the sphere to cross 1m length of the interaction vessel it takes 0.43 seconds.

CHAPTER 7- Experimental challenges

It is very essential to validate the numerical analysis for asserting the claim of certain scenarios and phenomena. This kind of validation can also be done with the help of commercial codes available in the nuclear industry. It will be more interesting if this validation is performed with small scale experimental facilities. The exciting part of the experimental validation is that we can directly visualize the MFCI effects with the help of digital imaging. Moreover, the debris particles can be observed directly which is the actual output of the experiment and can be used for supporting the theoretical analysis.

7.1 Approach for investigating MFCI effects:

Woods metal Facility (WM – Water system)

- Droplet and Stream fragmentation
- Debris bed forming characteristics
- Particle size spectrum & bed porosity

Sodium Fuel Interaction Facility (SOFI)

- Uranium melt – Sodium system
- Uranium Dioxide melt - Sodium system

Post Accident Thermal Hydraulics Facility (PATH)

- Assessment of natural convection in and around core catcher
- Simulation of dislocated core debris bed
- Design optimisation for enhanced fluid flow
- Demonstration of long term coolability of dislocated core under CDA thermal load

SOFI, Sodium Fuel Interaction test facility has been setup in IGCAR (India) to conduct various experiments related to sodium fuel interactions and to investigate the characteristics of melted fuel in liquid sodium. The main objective for this test facility is to investigate the debris bed profile, size characteristics and morphology subsequent to MFCI and to generate data in order for validating the mathematical models.

7.2 Challenges in SOFI Experiment:

- High temperature melting of Charge
  - U + SS @ 1600^0C
  - UO_2 + SS @ 3000^0C
- Simultaneous cooling of power supply, transformer and coil
- Integrity of crucible and its cooling
- Melt hold and release systems
- Isolation from sodium vessel

- Remote operation of various fast acting mechanisms
- Non contact temperature measurement
- Insulated melt guide path

7.3 Description of the SOFI Test Facility:

The overall layout and schematic of the test facility in shown in Figure 20. The facility is partitioned as three independent bays. The right bay consists of the SOFI Experimental setup, the middle bay consists of the control room and the left bay houses the cooling systems associated with the experimental setup. The SOFI experimental setup consists of three major modules, the top module which has the Cold Crucible Induction Melting System for melting core materials, the cooling circuit and melt releasing system. The intermediate module has a filter bucket with catcher plate inside an interaction vessel containing sodium along with argon cover gas system and then the bottom module has the dump vessel used for drainage of sodium.

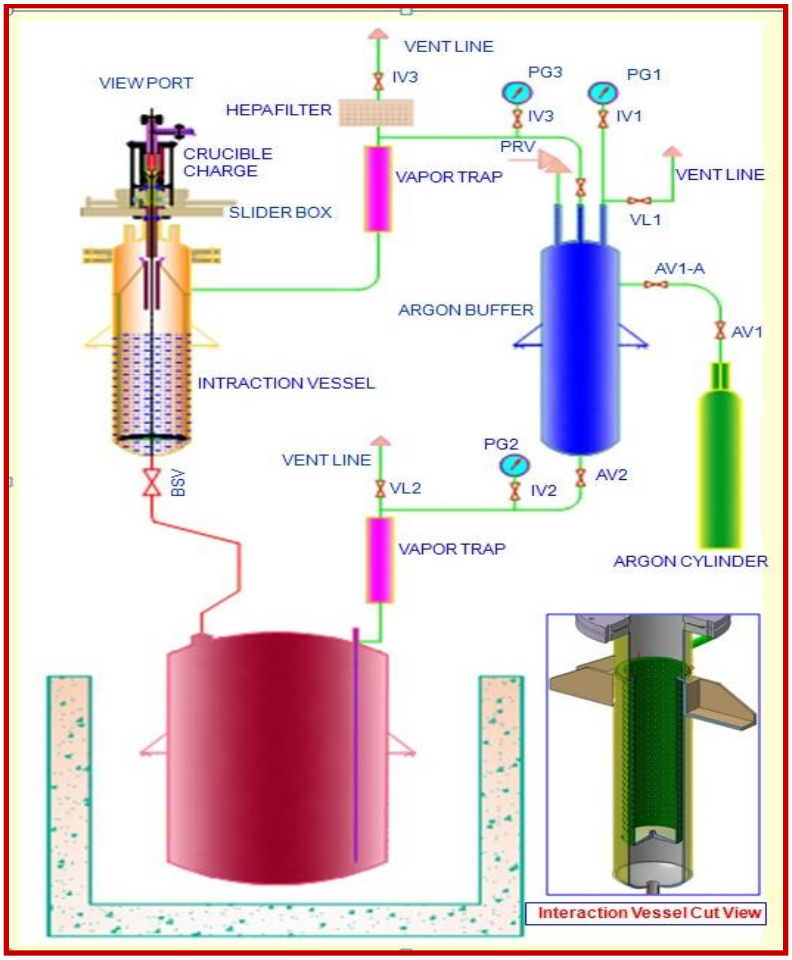

Figure 20: Schematic layout of the Test Facility (SOFI)

7.3.1 Top module components [Figure 20]:

i) The Induction heating system.

ii) Cold Crucible:

In the Cold Copper Crucible the charge is melted. The charge here refers to the fuel simulant that is to be melted for the experiment. It contains complimentary half section semicircular assemblies made of copper tubes. Each assembly comprises vertically oriented copper tubes mounted on semicircular square copper tubes both at the top and the bottom. The vertically oriented copper tubes are equally spaced between them. Each assembly has two inlets at the top and two outlets at the bottom for the coolant passage. These two semicircular assemblies are joined together to make a cylindrical copper tubing. To form a crucible this cylindrical copper tubing is coated with high temperature ceramic material (ZrO_2 paste) on the either side of the walls of the copper tubing. The bottom of the crucible consists of a ceramic tube which is used to discharge the molten fuel from the crucible.

iii) The associated cooling system:

A coolant has to be circulated around the crucible through the copper tubes in the crucible as well as inside the induction coil. This coolant is circulated by a pump and the process loop is shown in Figure 21. The coolant loop consists of an Oil tank, rotary gear pump, oil heat exchanger, inlet and outlet headers for flow distribution to crucible and induction coil. The oil is cooled by chill water in the oil heat exchanger and the chill water is circulated independent loop which consists of an air cooled water chiller which thus acts as a final heat sink. In order to cool the power supply system another independent cooling circuit is provided which circulates water through another air cooled water chiller. As the facility houses sodium, water and oil systems adequate precaution is taken by physically well separating the systems. This fact is clearly shown in Figure 21. The experimental bay can be seen in a 3 dimensional view in Figure 22 along with the picture of the cooling circuit bay.

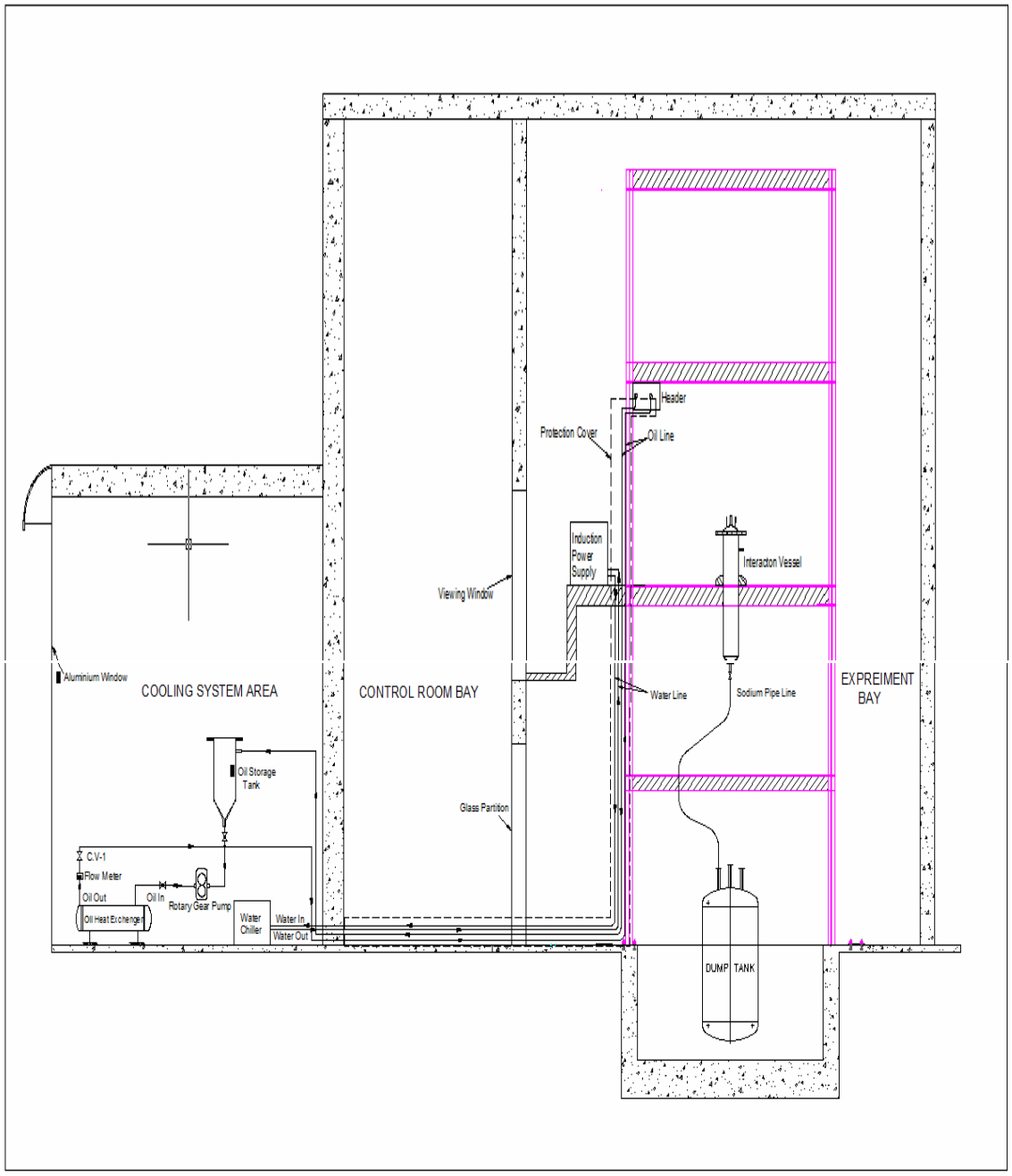

Figure 21: Sodium, water and oil systems of SOFI

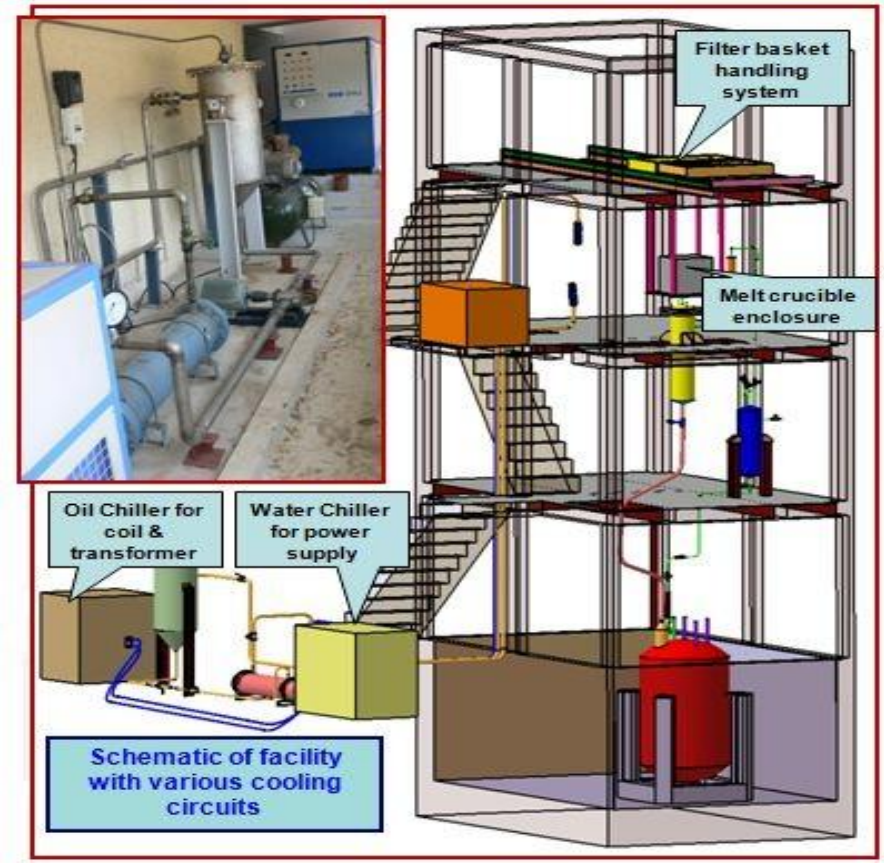

Figure 22: Layout of the SOFI Facility

7.3.2 Intermediate module components [Figure 20]:

-Interaction Vessel.

This vessel is designed to be loaded with solid sodium which is then heated upto 500^{o}C before the experiments are performed. During the experiment the molten fuel is drained from the crucible into the interaction vessel allowing the melt to interact with the liquid sodium within a filter bucket assembly kept in the vessel. After a run has been completed then the liquid sodium is allowed to cool back to handling temperature of atleast 200^{o}C and then completely drained back to the dump vessel under gravity allowing the removal of the filter bucket for the investigation of the fuel debris. The stainless steel interaction vessel is designed to accommodate 35kg sodium at 500^{o}C. This vessel is designed for an internal pressure of 10Bar at maximum temperature of 500^{o}C and checked for pressure of full vacuum at 200^{o}C. Additionally one vapour trap is also mounted on the interaction vessel at the argon line so that the sodium vapour is prevented from entering the cover gas circuit through argon gas lines. These vapour traps are fitted with surface heaters which are maintained at 200^{o}C so that the deposited sodium is drained back to the tank.

-Argon Buffer tank:

The argon buffer tank is designed to meet the requirements of both dump and interaction vessel for maintaining inertness required during operation and handling. This facilitates isolation high pressure argon cylinder from being directly connected to the sodium vessel and also acts as a buffer during the replacement of cylinders. This tank designed for an external pressure of 5Bar at maximum temperature of 200^{o}C.

7.3.3 Bottom module components [Figure 20]:

Sodium dump vessel is kept inside a pit. This is the major component of this module. This vessel is also connected with argon cover system so that the drained sodium from the interaction vessel remains in an inert atmosphere. This vessel is also designed to be used in the case of emergency. Sodium is generally drained to this tank after being cooled off to 200^{o}C after an experiment. This tank is provided with spark plug type discontinuous level probe for high level indication. This tank is designed to withstand an internal pressure of 5Bar at a maximum temperature of 500^{o}C and checked for full vacuum at 200^{o}C. Interaction vessels and drain vessels are provided with stainless steel sheathed MgO insulated expanded cold region type heaters. Sodium piping, valve and vapour traps are provided with quartz and ceramic insulated nichrome wire heaters.

In order to detect Sodium leaks a parallel wire type leak detectors made of nickel are provided at all welded joints of the drain vessel, interaction vessel, pipeline and valve. The valve is also provided with a spark plug type leak detector and for the sodium level measurements two discontinuous spark plug type level probes for high level indication and one discontinuous spark plug type level probe for low level indication are provided. The level probes are connected to the electronic circuit that sounds an alarm in case low levels.

7.4 Operating Procedure:

7.4.1 Charge melting and release system:

1) Crucible is loaded with required amount of charge (fuel simulant).
2) Close the crucible at the top with view port and connect the argon supply so that is charge melts in an inert atmosphere.
3) Coolant circulation through the crucible and induction coil.
4) Monitoring the flow rate of the coolant.
5) Switching on the induction power supply.
6) Increasing the power to maintain the heating rate at 20-40^{o}C/min.

7) Monitoring the temperature of the charge using the thermocouples placed on the charge itself and using radiation pyrometers mounted on the crucible.
8) Monitoring the temperature of the coolant on the outlet of the crucible and coil.
9) Once the required temperature (in this case being 1500^{o}C) is reached in the crucible, the melt is released to the interaction vessel.
10) After draining the melt from the crucible the slider valve is closed to isolate the interaction vessel from the crucible.
11) Switching off the induction power supply and then to stop the cooling systems after 10-15mins.

7.4.2 SOFI Experimental Data Parameters:

Melt Charge parameters

- Uranium (60 g) : Ø 10 mm x 40 mm
- Steel (500 g) : Ø 40 mm x 50 mm
- Melt temperature : 1600 ^{0}C
- Induction Power : 11 kW @ 7500 Hz

Cooling System parameters

- Oil temp at coil inlet and outlet : 21 ^{0}C and 87 ^{0}C (max)
- Oil flow rate : 4 lpm
- Air temp at crucible inlet and outlet : 27 ^{0}C and 51 ^{0}C (max)
- Air flow rate : 1000 lpm

Sodium System parameters

- Sodium temperature : 200 ^{0}C
- Amount of interacting sodium : 35 kg
- Height of interaction : 700 mm
- Catcher plate diameter : 170 mm
- Chimney height : 20 mm
- Chimney top cover : Ø 30 mm

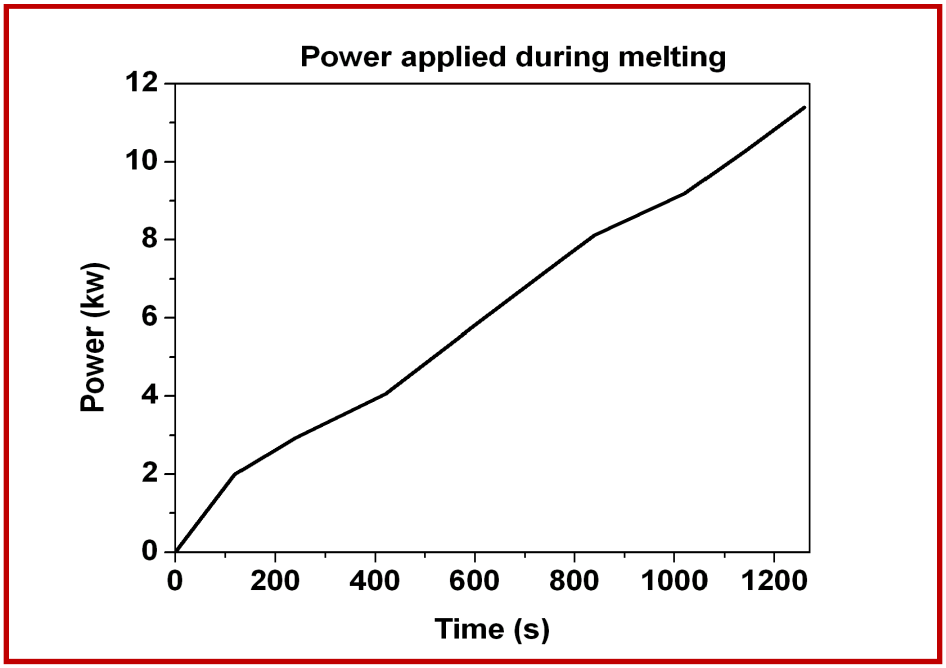

Figure 23: Power Applied vs Time

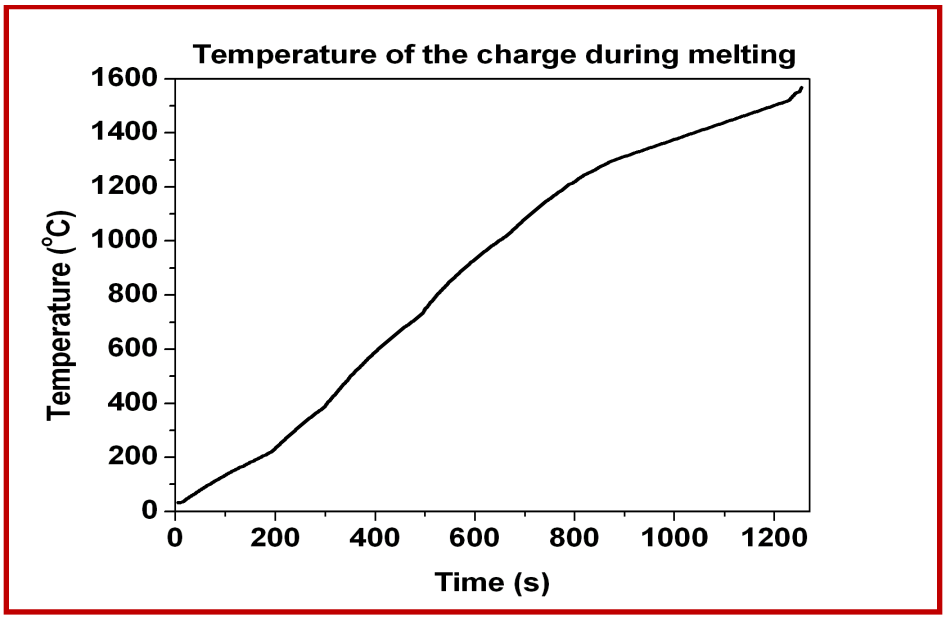

Figure 24: Charge temperature vs Time

Figure 23 shows the power applied to the induction coil from the start of the experiment till the melting of the charge inside the crucible is fully completed. The reason for providing this data is actually to explain one of the challenges faced during experiment and the solution that was developed. In a couple of runs initially, some variations in power application created certain

issues in the crucible and the coolant circuits. An optimum method of power application was then developed which yielded successful melting process. This is treated as an optimum range if we consider the shortest time possible for melting the charge. The power application can be much more gradual and slower, if there is no time constraint. The power increase leads to corresponding increase in the temperature of the charge which is shown in Figure 24.

7.5 Disposal Issues:

7.5.1 Cleaning of molten materials debris:

Molten material debris and filter bucket are cleaned for the removal of sticking of sodium. This cleaning process is carried out by using alcohols like ethanol. As the chemical reaction of ethanol with sodium is exothermic in nature and also this involves hydrogen gas generation, this cleaning process has to be carried out in a controlled manner under controlled atmospheric conditions in order to avoid the alcohol fire and hydrogen combustion. This cleaning process is generally carried out by the trained personnel only.

7.5.2 Radiological and Chemical Toxicity:

Radiological toxicity of uranium is mainly due to alpha radiation emission and it is primarily from the decay of U-238. As alpha radiation has a very short range and its inability to penetrate through paper, the working personnel are given sufficient protection in the form of gloves, masks and protective clothing.

CHAPTER 8- Discussion

8.1 Discussion:

In the process of MFCI (in our case, Uranium and Sodium), two regions are of high importance. Obviously, one is the Uranium side and the other is the process in the Sodium side.

In the sodium region, the convection process creates evaporation of coolant due to the initial high heat transfer from the hot molten sphere. Due to this evaporation the vapour expands within a short time registering a pressure pulse in the transducer. This pressure pulse is the deciding factor to predict the extent of the consequence during an accident scenario and the mechanical structure surrounding the core must be strengthened to accommodate the pressure developed and to suppress it. Thus in our calculation, the film pressure during interaction is analyzed and estimated in order to utilize this pulse value to design the structures in the future to avoid failure. From the analysis that have been performed the pressure generated in the interaction vessel for a mass of less than 2kg is well within the safety limits of the interaction vessel.

The other process of importance is the solidification occurring in the fuel region. The molten metal that is being cooled by sodium coolant will undergo solidification over a period of time and finally reaches the equilibrium temperature with the coolant where further temperature drop ceases. This time for reaching equilibrium is a critical parameter to obtain the state of the initial molten fuel at the bottom after settling. This solidification process can be divided into three time zones. The first is the temperature drop from molten superheat temperature to the freezing point of the metal then followed by a phase change at the freezing temperature to transform itself from liquid to solid uranium and at last the solid reduces its temperature to the condition of sodium. This total time is calculated using certain models given in the numerical analysis section. The velocity of this molten sphere once inside the liquid should be known. For this terminal velocity is calculated and assumed that at the instant of molten uranium touching the sodium, this terminal velocity comes into application thereby giving us an idea of how rapid the sphere settles to the bottom.

The calculation of terminal velocity yields 2.3m/s thus implying the time for fall of a 10mm diameter sphere is 0.43sec/m. The time for a 10mm diameter sphere for getting completely transformed into a solid is approximately 1.1 seconds. The interaction vessel in our experimental setup is of length 1m. Combining these values we can comment on the state of the molten metal. From the values, it is quite evident that the molten metal takes much longer time for transformation than the time for settling down. This makes us believe that the molten metal will be only partially solidified before it reaches the bottom and settles down. This scenario is not quite significant for smaller experimentation quantities like a few kilograms. This scenario if extends for a real condition, take in the case of an FBR, will be of high significance. If the initial molten sphere is only partially solidified on the core catcher, a chance of heap-shaped formation is probably high which can lead to considerable re-criticality situation. This is because the

quantity of fuel is enormous in a realistic system. This will surely lead to uncontrolled chain reaction and the risk of explosion. The calculation given in the numerical analysis section can be made for getting a preliminary idea of the condition on the core catcher. This analysis must be extrapolated to realistic conditions to deliver accurate predictions of the core catcher scenario and proper configuration of core catcher must be developed for preventing such conditions. The heat from the debris has to be removed completely and rapidly in the core catcher.

Figure 25 shows the debris after a successful Uranium+SS/Na interaction.

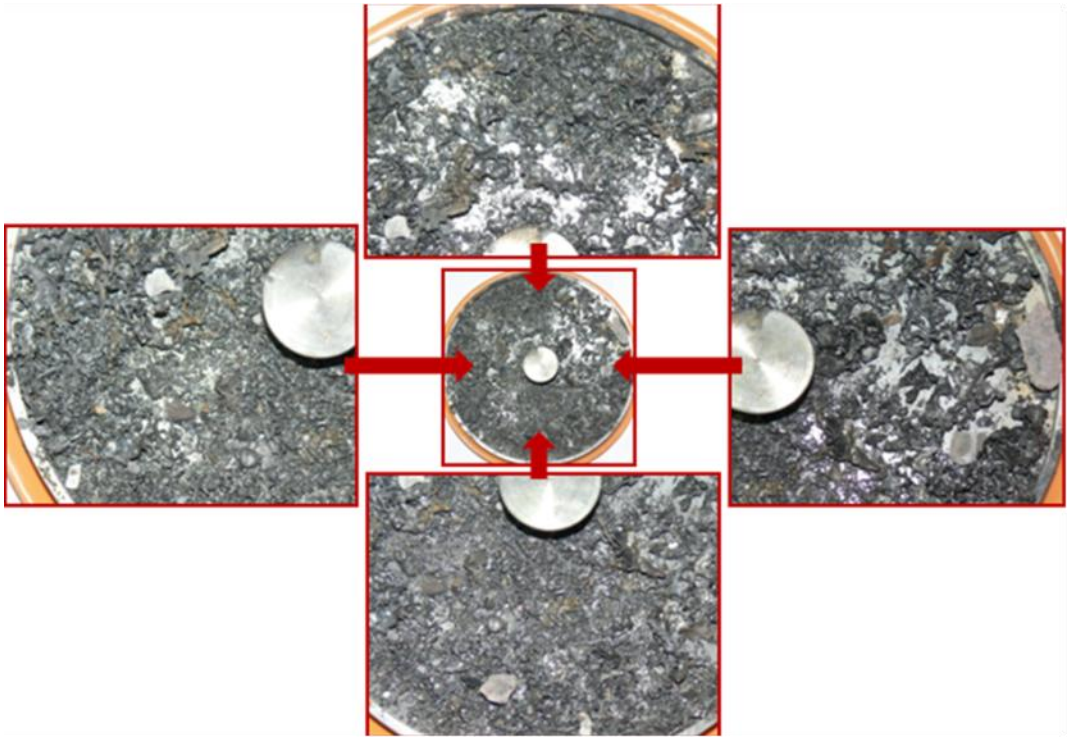

Figure 25: Uranium+SS debris after Sodium Interaction.

8.2 Future plan:

- In-sodium temperature measurement on melt travel path for online data

- In-sodium transient pressure measurement near to the interaction zone

- Dynamic imaging of debris fragmentation during the process in experiments

- Measurement of debris bed height on catcher plate using non-contact type sensors

- Increase of melt and sodium mass in stages for the next series of experiments

- Variation of interaction height in sodium as parameter

- Automation of filter basket handling for remote operation from control room

CHAPTER 9- Conclusion

9.1 Conclusion:

Consequences of whole core melt down were described briefly. The numerical and experimental activities completed towards investigating the mechanical consequences are addressed. Subsequently, thermal consequences, viz. molten coolant interactions (MFCI), core debris formation and settlement on the core catcher and post accident heat removal aspects were highlighted.

In the first phase, effects will be to simulate with Woods metal Facility in water system in the first phase, uranium melt in sodium system in second phase and uranium dioxide melt in sodium system in the third phase. The second and third phases will be simulated in SOFI facility. The Post Accident Thermal Hydraulics is studied using a dedicated facility called 'PATH' which has been recently commissioned at Safety Engineering Division (SED). For the PATH, the debris generated in the Woods metal in water system as subsequently debris collected from SOFI will be used for realistically simulated heat source and their thermal behaviour. The studies help to ensure adequate natural convection capability in the sodium pool, design optimisation for enhanced fluid flow and ultimately for demonstration of long term coolability of dislocated core under severe accident scenarios.

Molten Fuel and Coolant Interaction scenario being one of the most severe accident scenarios in an LMFBR, the analysis and experiments conducted in SOFI facility provides a basic knowledge of the phenomenon which occurs when molten fuel interacts with the liquid metal coolant in the containment vessel. From the analyses that have been performed it is evident that the interaction vessel used in the experiment has been with a high factor of safety. With more realistic and accurate assumptions it will be possible to design the containment vessel of a LMFBR for withstanding the MFCI accident and avoid failure during CDA.

The temperature history and the solidification front of the molten droplet have also been calculated and these calculations form the foundation of predicting the fragmentation phenomenon of the molten droplet in the sodium pool. The fragmentation process plays another vital role during MFCI and estimation of the extent of fragmentation yields an idea of the approximate condition of the molten core at the bottom of the containment vessel on the core catcher. The chances and probability of re-criticality depends on the state of the molten core on the core catcher which can be ultimately deduced.

References:

1. A.W. Cronenberg and H.K.Fauske: UO_2 solidification phenomenon associated with rapid cooling in liquid sodium, Argonne National Laboratory, USA, 1974.
2. Hiroshi Mizuta: Fragmentation of Uranium dioxide after molten uranium dioxide-sodium interaction, Power Reactor and Nuclear Fuel Development Corporation, 1974.
3. Roland B. Knapp and Neil E. Todreas: Thermal stress initiated fracture as a fragmentation mechanism in the UO_2-Sodium fuel-coolant interaction, Massachusetts Institute of Technology, USA, 1975.
4. H. Schins (JRC Ispra Establishment, Italy) and F. S. Gunnerson (University of Central Florida, USA): Boiling and Fragmentation behaviour during fuel-sodium interactions, 1985.
5. J. D. Gabor, R. T. Purviance, R. W. Aeschlimann and B. W. Spencer: Break-up and Quench of molten metal fuel in Sodium, Argonne National Laboratory, USA, 1988.
6. Satoshi Nishimura, Izumi Kinoshita, Nobuyuki Ueda (Central Research Institute of Electric Power Industry, Tokyo) and Ken-ichiro Sugiyama (Hokkaido University, Sapporo): Thermal Fragmentation of a molten metal jet dropped into a Sodium pool at Interface temperatures below its Freezing point, Japan, 2002.
7. Eiji Matsuo, Yutaka Abe (Graduate School of Systems and Information Engineering, Japan), Keiko Chitose (Mitsubishi Heavy Industries Limited, Japan), Kazuya Koyama (Mitsubishi FBR systems Inc., Japan) and Kazuhiro Itoh (Department of Mechanical and Systems Engineering, Japan): Study on Jet break-up behaviour at core disruptive accident for fast breeder reactor, 2007.
8. Louis C. Burmeister: Pressure excursions in transient film boiling from a sphere to a subcooled liquid, Mechanical Engineering Department, University of Kansas, USA, 1978.
9. L.Caldarola: A theoretical model for the molten fuel-sodium interaction in a nuclear fast reactor, Germany, 1972.
10. Frank P.Incropera, David P.Dewitt, Theodore L.Bergman, Adrianne S.Lavine: Fundamentals of Heat and Mass Transfer.
11. P.Vallet: The Physical Chemistry of Steel Making, 1958.
12. C.M.Adams: Trans Am. Society of Metals, Vol-50A, pg187, 1958.
13. J.Campbell: Hydrostatic tension in solidifying materials, British Iron and Steel research association, 1968.
14. Wikipedia
15. Internal safety report- Indira Gandhi Center for Atomic Research

Appendix I

k= thermal conductivity (w/mK) [for Uranium= 60.05W/mK, for Sodium= 69.54W/mK]

ρ= density (kg/m^3) [for Uranium=17300 kg/m^3, for Sodium= 860 kg/m^3]

c= specific heat capacity (J/kgK) [for Uranium=198 J/kgK, for Sodium= 1280 J/kgK]

Parameters for the calculation of interface film pressure

P_∞= pressure far from sphere (bar)= 1bar

p_m= maximum value of p

p= dimensionless total film pressure = P/P_∞

p_{v0}= dimensionless initial vapour pressure = P_{v0}/P_∞

α= dimensionless parameter

k_v= vapour thermal conductivity (W/mK)= 0.048W/mK

T_w= Sphere surface temperature (K)

T_∞= temperature far from sphere (K)

ρv_0= initial vapour density (kg/m^3) = 0.281kg/m^3

Λ= heat of vapourization (J/mol) = 96960J/mol

ρ= liquid density (kg/m^3) = 860kg/m^3

R= sphere radius

δ_0= initial film thickness

F= dimensionless parameter

τ= dimensionless time = At

τ_m= value of τ at pressure's first maximum

A= parameter, $A^2= P_\infty/R\rho\delta_0$

Parameters for calculating initial film thickness

$y= \delta_0 / R_f$

μ= viscosity of sodium vapour film= 2.6×10^{-4}dyne s/cm^2

λ_b= vapour thermal conductivity= 6.5×10^{-4}W/cmK

T_w= surface temperature of sphere

θ_s= saturation temperature of sodium= 1156K

ρ_b= density of vapour 0.281kg/m^3

L_{eq}= equivalent specific heat of vapourization

R_f= radius of sphere

g= acceleration due to gravity= 9.81m/s^2

ρ_f= density of fuel(kg/m^3)=17300kg/m^3

c_p= vapour specific heat capacity at constant pressure= 2.3×10^7erg/gK

1 dyne= 10^{-5}N

1erg= 10^{-7}J

Table for interface pressure developed and the corresponding time

Table 1

Mass	**72.5mg**	**1.95 g**	**9 g**	**70 g**	**0.570 kg**	**1.13 kg**	**1.95 kg**
Diameter of Melt	**2mm**	**6mm**	**10mm**	**20mm**	**40mm**	**50mm**	**60mm**
1700K; 673K	0.00062	0.0015	0.0024	0.0042	0.0076	0.0092	0.0107
Time	0.393μs	0.327μs	0.300μs	0.267μs	0.238μs	0.229μs	0.223μs
1700K; 573K	0.00055	0.0014	0.0021	0.0038	0.0067	0.0081	0.0095
Time	0.413μs	0.347μs	0.319μs	0.283μs	0.253μs	0.244μs	0.236μs
1600K; 673K	0.00047	0.0012	0.002	0.0032	0.0057	0.007	0.008
Time	0.433μs	0.360μs	0.331μs	0.295μs	0.263μs	0.253μs	0.246μs
1600K; 573K	0.00041	0.0010	0.0016	0.0028	0.005	0.0060	0.0070
Time	0.463μs	0.385μs	0.354μs	0.315μs	0.281μs	0.270μs	0.262μs
1500K; 673K	0.00035	0.00087	0.0013	0.0023	0.0042	0.0051	0.0059
Time	0.474μs	0.395μs	0.363μs	0.323μs	0.288μs	0.277μs	0.269μs
1500K; 573K	0.0003	0.00075	0.0011	0.0020	0.0036	0.0044	0.0051
Time	0.511μs	0.425μs	0.391μs	0.348μs	0.310μs	0.299μs	0.290μs